Physical and optical properties of young smoke from individual biomass fires in Brazil

Jeffrey S. Reid[1] and Peter V. Hobbs

Department of Atmospheric Science, University of Washington, Seattle

Abstract. Physical and optical characteristics of particles in smoke from 19 fires were measured in Brazil during the 1995 burning season as part of the Smoke, Clouds, and Radiation-Brazil (SCAR-B) project. The University of Washington C-131A measured particle sizes and absorption and scattering properties in very young smoke (<4 min old). These properties are related to fuel type, fire intensity, combustion efficiency, and particle composition. The count median diameter (CMD) of particles from tropical forest fires were strongly and positively correlated with the combustion efficiency. The particle volume median diameter (VMD) of the particles from forest fires did not correlate well with combustion efficiency, but it was highly correlated with the emission factors of particles and unsaturated hydrocarbons. The median diameter and standard deviation of the particle size spectra for smoke from grass and cerrado fires did not correlate with either the combustion efficiency or any emission factor. The measured particle radiative properties correlated well with the measured particle sizes and compositions, and the relationships between these parameters are described fairly well by Mie theory. The optical properties of smoke from individual biomass fires in Brazil differ significantly from those of smoke from biomass burning in North America. In particular, the total light-scattering coefficient for smoke particles in Brazil is, on average, 15% less than for smoke particles in North America. Also, the average values of the single-scattering albedos of smoke particles in Brazil are 0.05 to 0.1 less than those in North America.

1. Introduction

Biomass burning is a major source of pollutants, generating an estimated 104 Tg yr^{-1} of aerosol particles worldwide [*Andreae*, 1991]. These particles have been implicated in global radiative forcing [*Penner et al.*, 1992; *Intergovernmental Panel on Climate Change (IPCC)*, 1996; *Hobbs et al.*, 1997b] as well as global chemistry [*Andreae*, 1991]. Smoke plumes from the largest fires can cover thousands of square kilometers, resulting in noticeable decreases in surface temperatures and possibly even changes in atmospheric circulation [*Robock*, 1991; *Westphal and Toon*, 1991].

Eighty percent of the particles from biomass burning are generated in the tropics and, of these, one third originate in South America [*Andreae*, 1991]. While several recent studies have reported on the emission factors and chemical compositions of biomass-burning aerosols in Brazil [*Ward et al.*, 1992; *Artaxo et al.*, 1994; *Ferek et al.*, this issue], there are fewer data on the size distributions and optical properties of the smoke particles [*Anderson et al.*, 1996]. Most of the data on these latter parameters are for North American fires [*Radke et al.*, 1988,1991; *Hobbs et al.*, 1997a].

Smoke particles evolve rapidly after emission due to coagulation, outgassing, condensation, and gas-to-particle

conversion. For example, *Liousse et al.* [1995] measured particle growth in African savannah fire plumes within 50 m of the fire, and *Hobbs et al.* [1997a] and *Reid et al.* [this issue (a)] report on particle growth in smoke over periods from minutes to days. Thus the age of smoke particles can have a significant effect on their physical and chemical (and consequently radiative) properties.

In August and September 1995 the University of Washington (UW) Cloud and Aerosol Research group, with its Convair C-131A research aircraft, participated in the Smoke, Clouds, and Radiation-Brazil (SCAR-B) field project. One of the main goals of SCAR-B was to obtain measurements of the physical, chemical, and radiative properties of the palls of smoke which cover millions of square kilometers of the Amazon Basin and the cerrado regions of Brazil during the burning season.

Prior to studying particle aging, the properties of young smoke particles must be characterized; this is the purpose of the paper. We describe measurements, made aboard the C-131A aircraft, of the physical and optical characteristics of smoke particles between 2 and 4 min old. The properties of these young smoke particles were affected by coagulation and the condensation of vapors but not by photochemistry and cloud processing, which can affect older smoke particles. In a companion paper [*Reid et al.*, this issue (a)], we describe the properties of older smoke particles in regional hazes.

2. Background

Most biomass burning in Brazil occurs in two broad vegetation categories: cerrado and rain forest. The Brazilian cerrado covers 1.8 million square kilometers with a foliage composed of thick brush and semideciduous forest [*Coutinho,*

[1]Now at Propagation Division, Space and Naval Warfare System Center-San Diego, D883, 49170 Propagation Path, San Diego, California.

1990]. Plant communities can be loosely differentiated by foliage size, from low brush and grasses (campo sujo and campo cerrado) to forests with canopies as high as 10 to 20 m (cerrado sensu stricto and cerradao). While natural fires can occur in the cerrado region, the principal source of biomass-burning emissions are prescribed fires used to clear land for cattle and other land management purposes. During the SCAR-B project, smokes from prescribed and deforestation fires of cerrado vegetation were studied, as well as many grass (pasture) fires.

North of about 10°S in Brazil, the foliage is composed of rain and broadleaf deciduous forests (the Amazon Basin). In this region, fires are used as a land management tool for both primary deforestation and seasonal burning of secondary forests and pastures [Fearnside, 1990]. Biomass-burning rates in the Amazon Basin are not well quantified. However, current best estimates are 10^4 to 10^5 km^2 yr^{-1}, of which roughly one third to one half is deforestation [Fearnside, 1990, 1991; Kaufman et al., 1990].

The burning of vegetation can be broken down into two combustion phases: flaming and smoldering. In flaming combustion, hydrocarbons are volatized from the thermally decomposing biomass, mixed with air, and rapidly oxidized in a flame. Fire fuel components in the flaming phase are cellulose (50-65%), lignins (16-35%), extractives (0.2%-15%), minerals, and water. While the several hundred reactions involved in combustion are not completely understood, the general reaction can be approximated by the combustion of cellulosic fuels [Pyne, 1984]:

$$C_6H_{12}O_6 + 6O_2 \rightarrow 6CO_2 + 6H_2O + 1.26 \times 10^6 \text{ kJ}$$
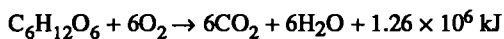
Flaming combustion starts when the temperatures of the biomass reaches a temperature where exothermic reactions can take place, which is about 610 K for a pilot flame and 880 K for spontaneous combustion [Chandler et al., 1983].

Particle formation begins with the creation of condensation nuclei, such as black carbon. Black carbon formation in a flame is generally restricted to combustion in the temperature range 1300-1600 K [Turns, 1996]. Current theories suggest that the particle formation process begins with the creation of large polycyclic aromatic hydrocarbons (PAH) from ejected fuel gases [Glassman, 1988]. The formation of cyclic molecules and PAH in the flame zone is believed to be closely linked to the availability of double- and triple-bonded hydrocarbons. Indeed, soot yields from alkanes are almost half those from their alkene and alkyne counterparts and one third those from aliphatic aromatics [Kent, 1986].

The PAH molecules grow to between 3000 and 10,000 atomic mass units through chemical and mechanical processes. At this point, these microparticles become condensation nuclei for other pyrolized species and experience considerable growth. Subsequently, many of these particles are oxidized in the interior of the flame zone. If insufficient air is transported into the flame, or if the temperature is not high enough to complete oxidation, many of these particles are emitted in the smoke.

The flaming phase expires when most of the volatiles have been expelled from the cellulose fuel [Chandler et al., 1983]; smoldering combustion then begins. Smoldering combustion is, in essence, a surface process, as oxygen diffuses to the surface and reacts exothermally with carbon at temperatures >710 K. If temperatures are increased to 910-980 K, CO can

convert to CO_2. The mass fraction of soot in aerosols produced in smoldering combustion is less than for flaming combustion. There have been few studies on aerosol formation in the smoldering phase, but it is known that the particles are formed by the condensation of volatalized organics [Ward, 1990].

The primary goal of this paper is to explore how smoke particle characteristics are related to measurable variables of fires: fuel type, the efficiency of combustion, and fire intensity.

Fuel type affects the properties of smoke particles because different fuels (e.g., grasses, shrubs, trees) have different mass loadings, surface area-to-volume ratios, and moisture contents. Because of the difficulty in characterizing fuel types from the air, fire fuels were divided into three broad categories: grass (or pasture), cerrado, and forest.

The second variable that affects smoke particles is the efficiency of combustion. Ward and Hardy [1991] define the combustion efficiency (CE) as the ratio of the concentration of carbon, [C], emitted as CO_2 to the total carbon emitted:

$$CE = \frac{[C]_{CO_2}}{[C]_{CO_2} + [C]_{CO} + [C]_{HC} + [C]_{PC}} \qquad (1)$$

where the subscript HC indicates the total unburned hydrocarbons (methane, nonmethane hydrocarbons (NMHC)), and PC the particulate carbon emitted. Thus CE is the fraction of fuel carbon emitted which is completely oxidized to CO_2. When CE $\gtrsim$ 90%, a fire is generally in the flaming phase, and when CE $\lesssim$ 90%, it is in the smoldering phase [Ward and Hardy, 1991]. The smoke emitted from most fires is a product of flaming and smoldering combustion and can thus be described as "mixed" phase. Environmental variables such as fuel size and moisture, wind speed, atmospheric relative humidity, and fire direction (i.e., heading or backing) all influence combustion efficiency [Ward et al., 1991].

Although the combustion efficiency defined by (1) is a very useful quantity for fire models, in experimental studies, it is often difficult to measure HC and PC. Since the emission of CO is closely linked to the emission of HC and PC [Ferek et al., this issue], in this study we will use the modified combustion efficiency (MCE), which is defined as [Ward and Hao, 1992]

$$MCE = \frac{[C]_{CO_2}}{[C]_{CO_2} + [C]_{CO}} \qquad (2)$$

Since NMHC and particulate carbon are emitted in relatively small quantities relative to CO_2 and CO, the difference between CE and MCE is typically only a few percent. Ferek et al. [this issue] show that for the SCAR-B data, CE=1.22 (MCE) - 0.22 (r^2=0.99).

The third variable that we will use to characterize fires is fire intensity. Ward and Hardy [1991] suggest that fires of higher intensity tend to emit larger particles. Also, it has been hypothesized that intense oxygen-starved combustion can have a significant effect on smoke particles [Cofer et al., 1997]. To test these hypotheses, we will attempt to relate fire intensity to particle properties.

Fire intensity is difficult to quantify. However, in this paper we wish simply to separate qualitatively the properties

of smoke particles generated by low-intensity and high-intensity fires. To this end, we employ two methods. First, we can relate particle properties to the NO_x emission factor of the fire. NO_x is produced in fires from fuel nitrogen and by the oxidation of molecular nitrogen at high temperatures [Lobert and Warnatz, 1993]. Emission factors for fuel nitrogen should reach peak values in early flaming combustion, where fuel temperatures are high. Similarly, thermally produced NO_x increases with increasing flame temperatures. In both cases, NO_x can be used as a surrogate for flame temperature, and we assume that flame temperature and fire intensity are linearly related.

The second method we used to estimate fire intensity involves the generation of a zeroth-order flux-intensity scale. Because over 90% of all carbon emitted from a fire is in the form of CO_2 and CO [Ferek et al., this issue], the rate of CO_2 + CO release is linearly related to the combustion rate of the fire and hence to the fire intensity. We assume that this scale is proportional to the flux rate of CO_2 plus CO at the surface. We start with the conservation of mass, namely, that the CO_2 + CO flux rate in a plume is constant at all altitudes ($c_c wA$=constant, where c_c is the concentration of CO_2 plus CO in ppm, w is the vertical velocity, and A is the cross section of the plume). Because most of our sampling was done in the central buoyant column of a smoke plume, we can use an axisymmetric thermal model to approximate smoke rise and entrainment. In this model, the radius of the horizontal dimension of the plume R is proportional to the plume height z [Scorer, 1978]. Thus $c_c wz^2$=constant. This yields a fire flux-intensity scale with units of ppm s^{-1}. We also use Scorer's relationship for the vertical velocity of a thermal puff: $w=1.2(gRB)^{1/2}$, where g is the acceleration due to gravity, and B is the buoyancy of the plume ($B=g\rho'/\rho_a=gT'/T_a$, where ρ_a and T_a are the ambient atmospheric density and temperature, respectively, and ρ' and T' are, respectively, the density and temperature perturbation in the plume). Because the range of values of the flux-intensity scale defined in this way varies over 2 orders of magnitude, we use the logarithm to the base 10 of the flux-intensity scale.

3. Instrumentation and Sampling Techniques

The instrumentation aboard the University of Washington (UW) Convair C-131A in SCAR-B, the flight paths, and summaries of the accomplishments of each flight are given by Hobbs [1996]. Therefore we give here only brief descriptions of the instrumentation and experimental techniques pertinent to this paper.

The UW C-131A had aboard instrumentation for both continuous and intermittent "grab-bag" sampling. Much of the aerosol and some of the gas instrumentation could not react quickly enough to properly resolve the high concentration gradients present in plumes close to the fires. Therefore we employed a "grab-bag" technique, in which a 2.5 m^3 Velostat bag was rapidly filled with a sample of the smoke by ram air pressure. Samples for filters, particle sizing, and some gas measurements were obtained from the grab bag. These measurements were correlated to data from the continuous sampling instruments averaged over the time period for which the grab-bag sample was collected. The grab-bag system had an aerosol cut point diameter of roughly 4 μm (PM$_4$).

Over the 12 s that it takes to fill the grab bag, the aircraft travels about 960 m. All of the measurements presented in this paper were derived from a sample collected across the width of a smoke plume. Therefore the measurements can be interpreted as averages across the width of a plume. On some occasions, two passes through a plume (separated by less than 2 min) were required to fill a bag. Some ambient air (<25% by volume) was generally collected in a grab-bag sample. However, since aerosol mass concentrations in the smoke plumes ranged from 5 to 50 times greater than in the ambient air, the influence of ambient air on the intensive properties of the plume samples was small (<10%).

Gas measurements made on the C-131A aircraft included CO_2, CO, NO_x, NO, SO_2, O_3, and certain hydrocarbon concentrations. The instruments used to measure CO_2, NO_x, and O_3 had short enough response times to permit continuous sampling during a plume penetration. In addition, a valve on the continuous gas analyzer manifold could be briefly switched to the bag to obtain measurements of CO_2 of NO_x of a bag sample. The CO and SO_2 measurements were strictly from the grab-bag samples. A discussion of the hydrocarbon emission factor data used in this paper is given by Ferek et al. [this issue].

Teflon filters exposed to grab bag samples were gravimetrically analyzed in a humidity-controlled chamber to ±6 μg accuracy (±1 μg precision) to determine the mass concentration of the dried aerosol. In comparison, the average filter loading was 100 μg. These filters were subsequently analyzed by ion exchange chromatography for the following ions: Cl$^-$, NO_2^-, NO_3^-, $C_2O_4^{2-}$ (oxalate), SO_4^{2-}, Ca^{2+}, K^+, Mg^{2+}, Na^+, NH_4^+. Quartz filters were analyzed for total carbon and black carbon concentrations in the aerosols using the technique of Cachier et al. [1989]. A discussion of particle composition is given by Ferek et al. [this issue].

Two instruments were used to size particles in high concentration in the smoke plumes: a differential mobility particle sizer (DMPS) and the PMS forward scattering spectrometer probe 300 (FSSP-300). The DMPS provides aerosol size spectra from 0.01 to 0.6 μm diameter based on particle electromobility [Winklmayer et al., 1991]. Since this instrument requires a 2 to 4 min analysis time, it was fed from the grab bag. During collection, particles were slightly dried (RH drops by <15%) due to higher temperatures inside the aircraft cabin. However, for the results presented in this paper the ambient relative humidity was not high enough to cause much hygroscopic growth of the particles [Kotchenruther and Hobbs, this issue]. The DMPS had a 310°C preheater, which could be used to bake off volatile compounds (such as organics, sulfate, nitrate, and tightly bound water) from the sample aerosol. After applying this thermal pretreatment, the DMPS was used to measure the size spectrum of the remaining nonvolatile components of the particles.

DMPS number distributions were parameterized by a lognormal curve fit:

$$dN = \frac{1}{\sqrt{2\pi} \ln \sigma_{gc}} \exp\left[-\frac{\left(\ln d_p - \ln \text{CMD}\right)^2}{2\left(\ln \sigma_{gc}\right)^2}\right] d\left(\ln d_p\right) \quad (3)$$

where d_p is the particle diameter, dN is the number of particles in a $d(\ln d_p)$ interval, CMD is the count median diameter, and σ_{gc} is the geometric standard deviation of d_p. A similar

expression was used to parameterize aerosol volume distributions:

$$dV = \frac{1}{\sqrt{2\pi}\ln\sigma_{gv}}\exp\left[-\frac{\left(\ln d_p - \ln \text{VMD}\right)^2}{2\left(\ln\sigma_{gv}\right)^2}\right]d\left(\ln d_p\right) \quad (4)$$

where dV is the volume of particles in a $d(\ln d_p)$ interval, VMD is the volume median diameter, and σ_{gv} is the geometric standard deviation of the volume distribution.

The FSSP-300 was used to measure particles with diameters from 0.3 to 20 μm. In this instrument, sizing is based on the forward scattering of light by the aerosol relative to a polystyrene standard aerosol. Thus the FSSP-300 is prone to slight sizing biases for aerosols with low single-scattering albedos or indices of refraction significantly different from polystyrene (1.59). On the other hand, since the FSSP-300 is an open-celled instrument mounted on the wing of the aircraft, it has the advantage of providing in situ measurements of the particle size spectrum.

Intercomparison of the particle sizes measured on the C-131A in SCAR-B shows some differences between the particle size distributions measured by the DMPS and the optical probes such as the FSSP-300 [*Reid et al.*, this issue (a)]. The DMPS and the optical probes on the C-131A generated nearly identical count distribution functions in the size range where they overlap. However, in regional haze samples, *Reid et al.* [this issue (a)] found that the VMD and σ_{gv} derived from the DMPS measurements were systematically higher than those derived from the optical probes. The differences in the VMD values were up to 0.05 μm. This discrepancy is likely due to differences between particle mobility and optical equivalent diameters, as well as the required inversion performed on DMPS data. Since the data from the different instruments were linearly correlated, the relationship between the equivalent electrical mobility diameter and the optical equivalent diameter of smoke particles was established [*Reid et al.*, this issue (a)].

The absorption properties of the smoke aerosol were measured using several techniques. A brief description of the relevant methods is given below; a complete discussion is given by *Reid et al.* [this issue (b)].

Aerosols collected on the Teflon filters were gravimetrically analyzed to determine aerosol mass concentrations (c_m). These filters were then subjected to integrating plate analysis [*Lin et al.*, 1973] to determine the aerosol absorption coefficient (σ_a) at a wavelength of 550 nm. Corrections were made for particle loading and multiple reflections in the filter substrate. Since the absorption measurements were performed in the laboratory, the values of σ_a are for dried particles. From measurements of σ_a, a bulk aerosol mass absorption efficiency (or specific absorption), α_a, can be obtained:

$$\sigma_a \equiv \alpha_a c_m \quad (5)$$

The determination of α_a is important because, when established, atmospheric absorption can be inferred from aerosol mass measurements (c_m).

From measurements of σ_a and the atmospheric light-scattering coefficient σ_s (from a nephelometer), the aerosol single-scattering albedo (ω_o) is obtained from

$$\omega_o \equiv \frac{\text{light scattering coefficient}}{\text{light extinction coefficient}} = \frac{\sigma_s}{\sigma_s + \sigma_a} \quad (6)$$

Single-scattering albedos were also derived more directly using measurements from an optical extinction cell (OEC). The OEC aboard the UW C-131A is, in effect, a 6.4 m long transmissometer [*Weiss and Hobbs*, 1992]. It provides direct measurements of the atmospheric extinction coefficient ($\sigma_e \equiv \sigma_s + \sigma_a$) by measuring the attenuation of a light beam (at a wavelength of 538 nm) that passes through a 6.4 m long tube containing a sample of the aerosol. An adjoining integrating nephelometer simultaneously measures σ_s; ω_o is derived from (3). When deriving ω_o, the slight difference in the wavelength employed by the IP and OEC (550 nm versus 538 nm) is not significant (<0.005).

The OEC does not dry the sampled particles; slight fluctuations in the sample temperature and relative humidity can, in principle, change the sizes of the particles. However, this is not an issue here since *Kotchenruther and Hobbs* [this issue] have shown that aerosols from biomass burning in Brazil have very low humidification factors (~1.15).

The light-scattering coefficient was measured in smoke plumes using an MRI 1567 integrating nephelometer operating at a wavelength of 550 nm. The inlet to the nephelometer on the aircraft was heated so that the relative humidity in the measurement cavity was <35%. Thus σ_s values are for the dry aerosol. This instrument has a fast response time (<1.5 s) and is therefore suitable for plume sampling. A small correction was made to account for truncation error and the slight non-Lambertian nature of the nephelometer.

To retrieve the wavelength dependence of the aerosol scattering, the UW C-131A was equipped with a three-wavelength (3-λ) nephelometer built by MS Electron [*Hegg et al.*, 1996]. This instrument measures total light scattering and back scattering at wavelengths of 450, 550, and 700 nm. Since the 3-λ nephelometer has a relatively long response time (~5 s), it cannot resolve fine details in plume structure; instead it measures light scattering averaged over the width of a plume. From these measurements the wavelength dependence of light scattering can be determined.

The MS Electron 3-λ nephelometer has a backscatter shutter to determine the total hemispheric backscatter ratio (90°-170°). This value represents the atmospheric backscatter fraction in an optically thin atmospheric smoke layer with the Sun directly overhead (not to be confused with the fraction of radiation scattered upward by aerosols in the atmosphere).

From the average σ_s, measured during the period the grab bag was open, the aerosol mass scattering efficiency (α_s) can be derived from

$$\sigma_s \cong \alpha_s c_m f(\text{RH}) \quad (7)$$

where c_m is the aerosol mass concentration from the grab bag, and $f(\text{RH})$ is the humidification factor $f(\text{RH})$. In (7), $f(\text{RH}) = 1$ because the measurements were made on dried aerosols. The aerosol mass scattering efficiency is a useful parameter since it can be used to estimate aerosol mass concentration from scattering measurements (and vice versa). Also, it allows a linkage between well-defined and frequently measured emission factors of fine particles ($d_p < 4$ μm) from fires and their influence on atmospheric light scattering.

The wavelength-dependent light-scattering coefficient also yields information on particle size characteristics through the Angstrom coefficient α:

$$\alpha \equiv -\frac{\ln\left(\sigma_e(\lambda_1)/\sigma_e(\lambda_2)\right)}{\ln\left(\lambda_1/\lambda_2\right)} \quad (8)$$

The Angstrom coefficient is often interpreted as being linearly related to the Junge distribution. Thus an increasing value of α implies a narrowing of σ_{gc}. From the 3-λ nephelometer measurements we can derive the Angstrom coefficient for two wavelength intervals: 450-550 nm and 550-700 nm. Since we do not have wavelength-dependent measurements of absorption, we derived values of α using the scattering portion of extinction (i.e., we assume $\sigma_e = \sigma_s$). While this changes the value of α, the qualitative relationship between α and the slope of the Junge distribution is not substantially affected.

4. Results

4.1. Overview

Flights were carried out between August 13 and September 25, 1995, during the height of the biomass-burning season in Brazil [*Artaxo et al.*, 1994]. To sample fires from several different regions and foliage types, the UW C-131A flew missions out of four locations in Brazil: Brasilia (the national capitol) and Cuiabá (Mato Grosso) in the cerrado region and Porto Velho (Rondonia) and Marabá (Pará) in the rain forested areas.
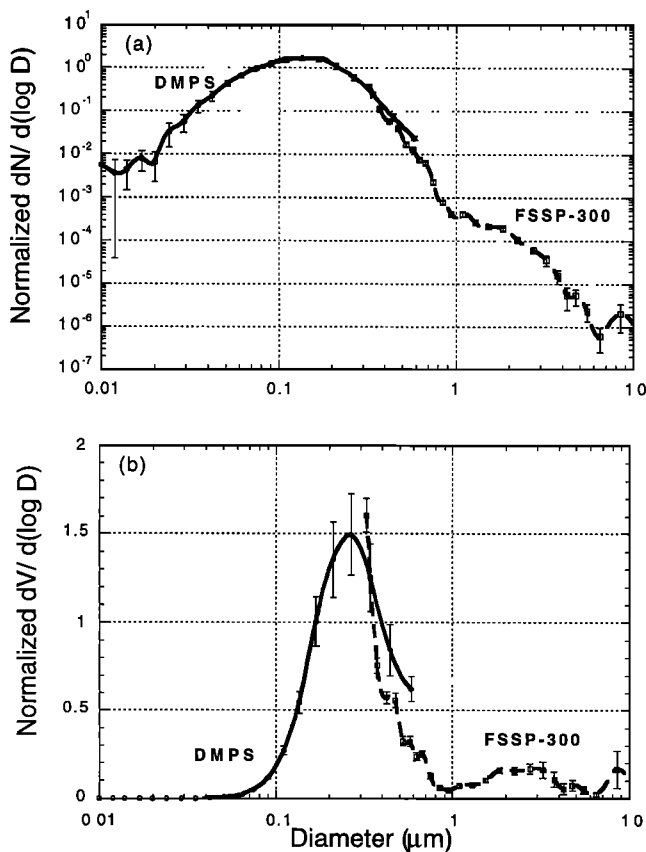
Figure 1. Average particle number (a) and volume (b) size distributions for all plume samples in Brazil. Vertical lines show standard errors in the mean value. The solid and dashed lines are measurements from the differential mobility particle sizer (DMPS) and forward scattering spectrometer probe 300 (FSSP-300), respectively.

Over 30 forest, cerrado, and grass fires were studied, with smoke samples taken from several hundred penetrations of smoke plumes. For a sample to be considered suitable for analysis it had to meet certain selection criteria, including (1) availability of filter, CO_2, CO and NO_x measurements; (2) the smoke sample was not more than about 4 min old; (3) sampling altitude <1000 m above ground level (agl), or ~1100 m agl for particularly large fires; and (4) the plume was not substantially diluted. Of the 30 smoke plumes observed, 19 met all of these criteria.

Twelve smoke samples from 10 forest fires (six flaming and six smoldering) were analyzed. Three of the fires were in the vicinity of Porto Velho and seven near Marabá. Fuel for the fires varied from slash to standing forest. Smoke samples were obtained, on average, at an altitude of ~360 m agl (965 hPa). Modified combustion efficiencies varied from 0.84 to 0.98. Excess particle mass (PM$_4$) concentrations in the plumes ranged from 200 to 3400 $\mu g \ m^{-3}$. No correlation existed among the aerosol mass concentration, MCE, and sampling height.

Six smoke samples were studied from five grass (pasture) fires: two in Brasilia, one in Porto Velho, and two in Marabá. Because of the nature of the fuel (small and dry) the MCEs were >90%, with an average of 95%. Smoke samples were collected on average at 480 m agl (950 hPa), with the highest at 880 m. Excess particle mass (PM$_4$) concentrations in these smoke plumes ranged from 130 to 500 $\mu g \ m^{-3}$.

Six smoke samples were obtained from four cerrado fires. One of the fires was just outside of Brasilia; the other three were in the vicinity of Cuiabá. Like the grass fires, the MCEs for the cerrado fires were high, averaging 94%. Sampling heights averaged 900 m agl (900 hPa), with the highest at 1078 m. Excess particle mass concentrations in the plumes varied from 60 to 450 $\mu g \ m^{-3}$.

4.2. Particle Structures and Size Distributions

To illustrate the basic nature and variability of the size distributions of particles produced by biomass burning in Brazil, average particle number and volume size distributions, based on all the data, are shown in Figure 1. The number and volume distributions for each plume were normalized to unity. By comparing the area under the curves to the measured mass concentrations, the average density of the smoke particles was found to be 1.35 ± 0.15 g cm^{-3}.

From Figure 1b we see that the submicron aerosol mode was dominant, accounting for over 90% of the total particle volume. This mode was dominated by particles produced by the combustion process. Over 85% of the mass in this mode was composed of organic compounds, with the remaining 15% being black carbon (7%), potassium (4%), and other elements (4%) [*Ferek et al.*, this issue]. A transmission electron microscopy (TEM) micrograph of particles collected in a typical forest fire shows the internal structure of the particles (Figure 2a). From this image we see that the constituents of the aerosols are both internally and externally mixed, and both single (roughly spherical) particles and aggregates are present. Most of the spherical particles had volatile shells covering one or more involatile core particles. The volatile shells were most likely organics.

Figure 2b shows an enlargement of a portion of Figure 2a. To enhance the fine structure of the particles, the negative image is shown in Figure 2b. Several aggregates (probably
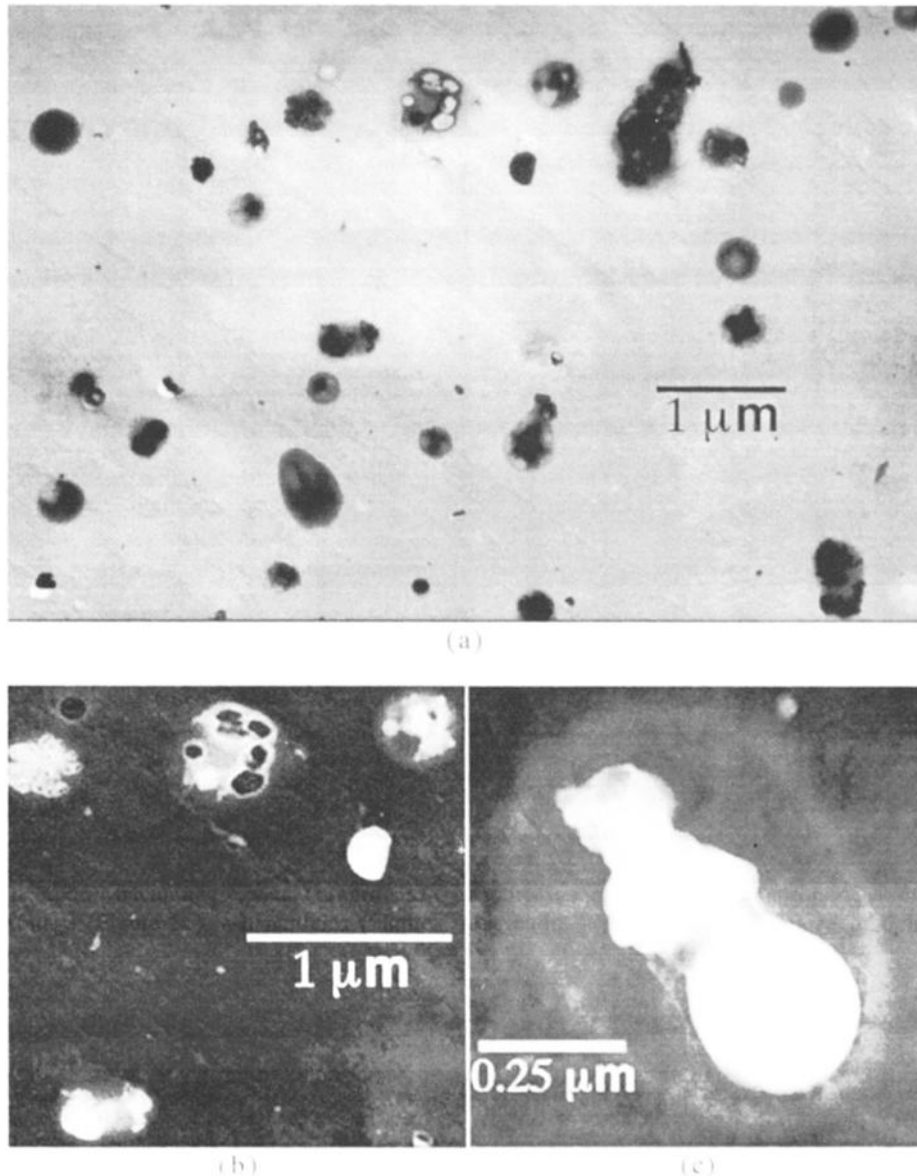
Figure 2. Transmission electron microscopy (TEM) micrographs of fine particles collected in the smoke plume from a mixed-phase forest fire in Brazil. (a) Low magnification view. This is a positive image, so darker areas indicate higher density material. Note the gray areas around the core particles where material has evaporated. (b, c) Digitally enhanced and enlargements of individual particles. Here the image negative is displayed. Thus lighter areas are denser material.

black carbon) with volatized shells are seen. An enlargement of another heterogeneous particle is shown in Figure 2c (also a negative image). Here a large "residue" ring is seen (this is likely to be somewhat larger than the original size due to flattening of the particle on impaction). The majority of the original particle has volatized, leaving the involatile core. The core particle itself is made up of several particles, probably BC and low volatility organics.

Figure 1b shows a second prominent volume mode between 1-4 μm diameter and a third mode near 9 μm that extended to 14 μm (not shown because of poor counting statistics). Scanning electron microscopy (SEM) micrographs of these particles (Figure 3) show them to be quite different from the submicron particles. They consist of carbon aggregates (Figure 3a), partially combusted foliage (Figure 3b), ash particles (Figure

3c), and soil (Figure 3d). These particles are similar to those found by Radke et al. [1991] in the smoke plumes from boreal fires. Small noncombustible matter on (or in) the foliage, such as soils on leaves or silicates in stems, are likely to be suspended into a fire plume. Also, soil particles can be suspended by saltation of surface dust driven by winds generated by the fire [Radke et al., 1991]. Particles such as these can have equivalent mass and aerodynamic diameters over an order of magnitude smaller than their geometric diameters, and the relationship between the geometric and the equivalent optical diameters is uncertain [Reid et al., 1994]. Thus even though such particles may account for 10% of the measured particle volume, their contributions to the mass, absorption, and scattering properties of the aerosol are uncertain. However, since coarse particles have low mass
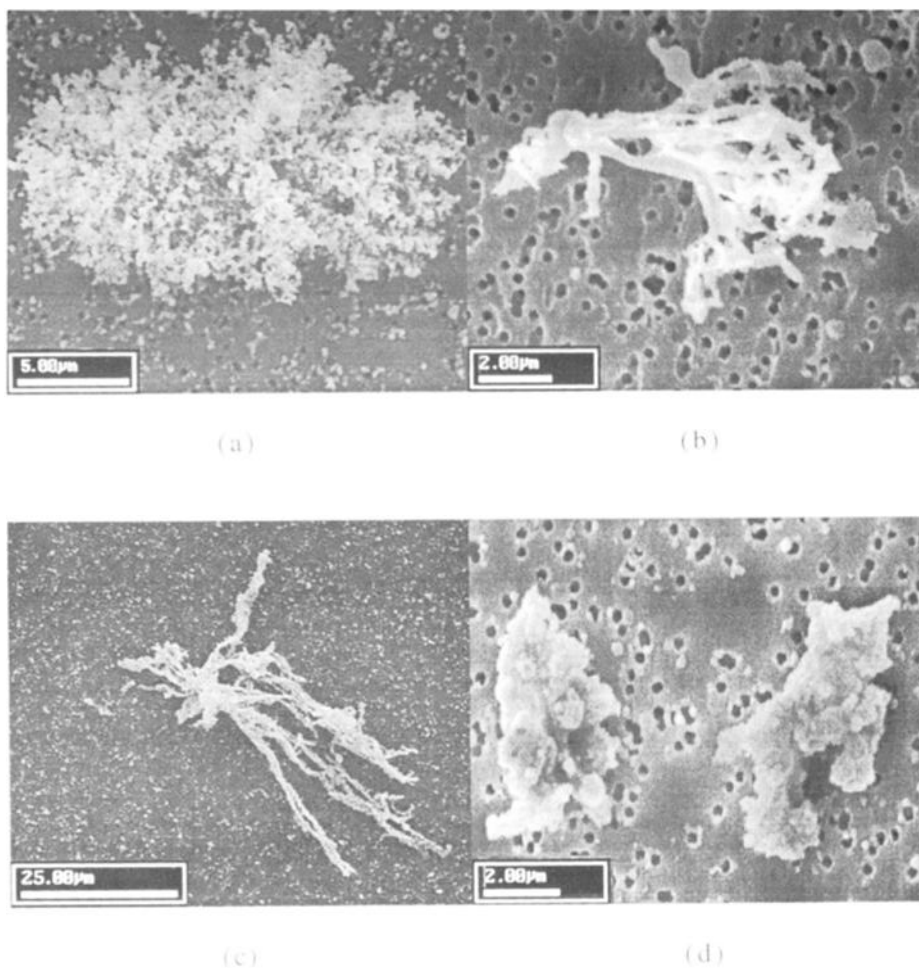
Figure 3. Scanning electron microscopy (SEM) micrographs of coarse particles collected from mixed-phase forest fires in Brazil. (a) Ash aggregate, (b) combusted plant fiber, (c) elongated ash particle, (d) soil particle.

scattering efficiencies, their impact on light scattering in the visible wavelengths is probably low.

There were considerable variations in the structure of the particle size distributions with regard to fuel, combustion efficiency, and other fire properties. A summary of the particle size characteristics by fuel type is given in Table 1. We will now discuss these results for each fuel type.

4.2.1. Forest fires. Average DMPS size spectra for flaming and smoldering forest fires are shown in Figure 4. From these distributions, two statistically significant trends are evident: CMD increases with increasing MCE, and the standard deviations of the number and volume distributions (σ_{gc} and σ_{gv}, respectively) decrease with increasing MCE. The first result is consistent with that reported by *Hobbs et al.*

**Table 1.** Particle Size Parameters (Mean ± Standard Error) for Smoke Less Than 4 min Old in Brazil

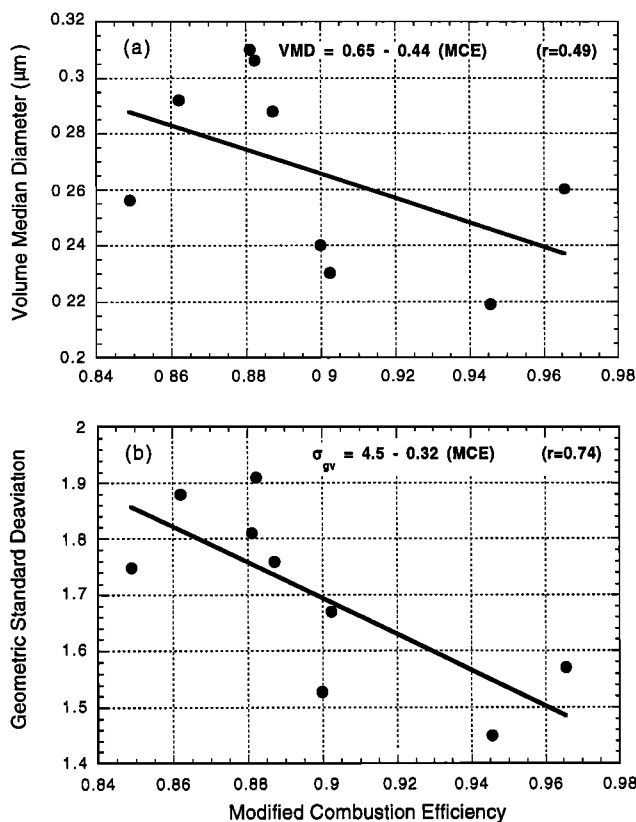|	Forest			
	(Flaming)	(Smoldering)	Grass	Cerrado
Particle Number Distribution				
Median diameter (μm)	0.13 ± 0.005	0.10 ± 0.005	0.10 ± 0.01	0.10 ± 0.01
Geometric standard deviation (σ_{gc})	1.68 ± 0.02	1.77 ± 0.02	1.79 ± 0.05	1.91 ± 0.15
Core median diameter (μm)	0.08 ± 0.02	0.05 ± 0.005	0.06 ± 0.01	0.06 ± 0.01
Core geometric standard seviation (σ_{gc})	1.80 ± 0.05	1.99 ± 0.04	1.95 ± 0.09	1.81 ± 0.08
Particle Volume Distribution				
Median diameter (μm)	0.24 ± 0.01	0.29 ± 0.01	0.30 ± 0.04	0.23 ± 0.02
Geometric standard deviation (σ_{gc})	1.62 ± 0.07	1.84 ± 0.05	1.87 ± 0.07	1.80 ± 0.14
Core median diameter (μm)	0.19 ± 0.02	0.18 ± 0.01	0.16 ± 0.02	0.13 ± 0.01
Core geometric standard deviation (σ_{gc})	1.65 ± 0.11	1.76 ± 0.17	1.59 ± 0.05	2.00 ± 0.2
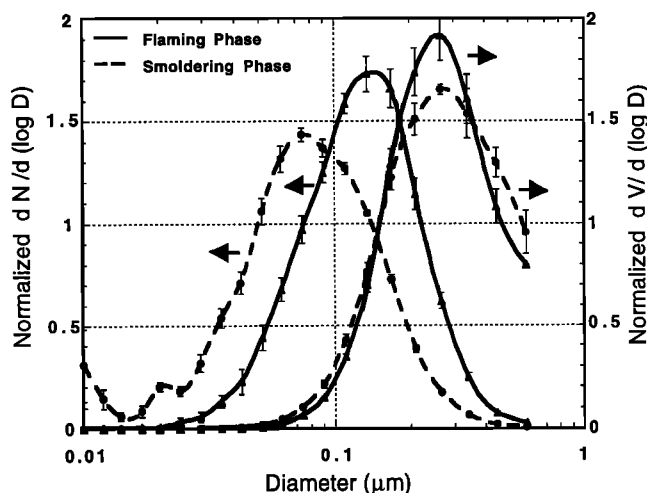
Figure 4. Normalized accumulation mode number and volume particle size distribution for aerosols produced by flaming (solid) and smoldering (dashed) forest fires in Brazil.

[1997a] for prescribed fires in the Pacific Northwest, but it differs from *Einfeld et al.* [1991] results for a prescribed fire in Montana. However, our relationship between the CMD and the MCE is strong (Figure 5a), with a correlation coefficient of 0.83.

The geometric standard deviation of the particle number distribution decreases with increasing combustion efficiency
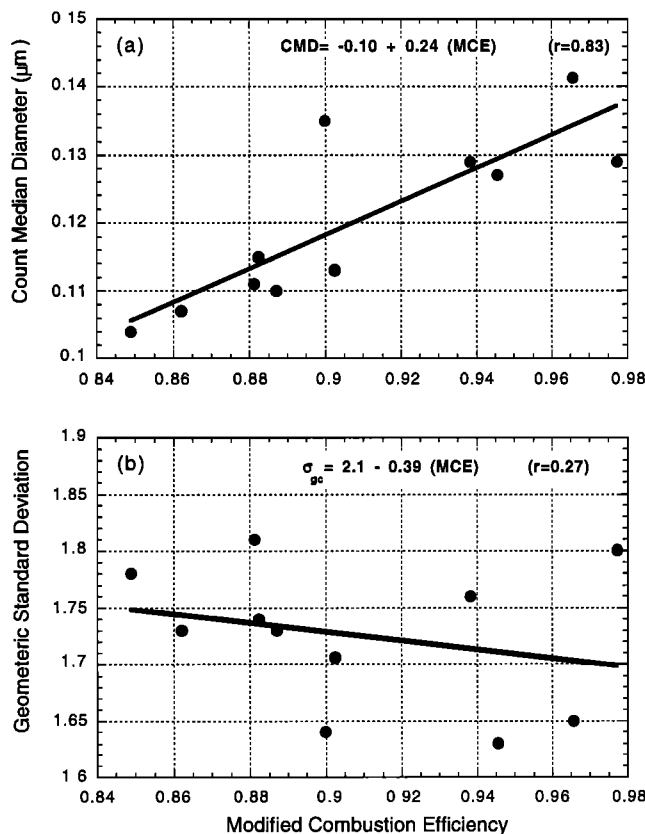
Figure 5. (a) Count median diameter and (b) geometric standard deviation of accumulation-mode aerosol in smoke from forest fires in Brazil versus the modified combustion efficiency.

Figure 6. (a) Volume median diameter and (b) geometric standard deviation of accumulation-mode aerosol in smoke from forest fires in Brazil versus the modified combustion efficiency.

(Figure 5b). This, in turn, gives rise to a slight decrease in particle VMD with increasing MCE (Figure 6a). This agrees with the results of *Einfeld et al.* [1991]. Like σ_{gc}, σ_{gv} is negatively correlated with the MCE. It is surprising that unlike the CMD, the VMD does not show a strong correlation with the MCE. However, because of the relatively few data points, the regression is not statistically significant at the 95% confidence level.

The relationships between the particle size distribution parameters and the MCE are somewhat puzzling. Current theories, supported by some data, suggest that the CMD, VMD, σ_{gc}, and σ_{gv} should all be strongly anticorrelated with the MCE [*Einfeld et al.*, 1991; *Radke et al.*, 1991]. To explore this, we correlated the particle number and volume distribution moments with the CE, MCE, the logarithm of the flux-intensity scale, and the emission factors for particles and gases. The correlations and p values are listed in Table 2.

As noted earlier, the CMD was highly correlated with the MCE. Therefore it is also well correlated and anticorrelated with the emission factors for CO_2 and CO, respectively. Also, a reasonable anticorrelation exists between the CMD and the NMHC, since these are highly correlated with CO. Thus those aspects of a fire that determine the MCE (such as fuel type, oxidation rate, fire intensity, and fuel-air ratio) are also likely to determine the CMD. As noted in section 2, particles are nucleated in flames by PAHs, and they grow by condensation and coagulation. In such high temperature and particle-rich environments, coagulation and condensation are essentially the same process because of the very small sizes of the

Table 2. Correlations and p Values (in Parentheses) of Particle Size Distribution Parameters (CMD, σ_{gc}, VMD, and σ_{gv}) With Three Fire Parameters (CE, MCE, and Flux-Intensity Scale) and Emission Factors for Nine Samples of Smoke From Flaming and Smoldering Forest Fires in Brazil

	CMD	σ_{gc}	VMD	σ_{gv}
Fire Parameters				
CE	0.82	-0.24	-0.46	-0.51
	(0.002)	(0.478)	(0.208)	(0.128)
MCE	0.83	-0.27	-0.48	-0.54
	(0.001)	(0.430)	(0.183)	(0.103)
	0.41	-0.75	-0.83	-0.91
Log of flux-intensity scale	(0.300)	(0.033)	(0.006)	(0.003)
Emission Factors				
Aerosol mass (PM$_4$)	-0.29	0.56	0.67	0.54
	(0.413)	(0.112)	(0.048)	(0.105)
CO$_2$	0.81	-0.66	-0.56	0.61
	(0.003)	(0.053)	(0.117)	(0.059)
CO	-0.83	0.61	0.15	-0.53
	(0.002)	(0.080)	(0.477)	(0.109)
NO$_x$	0.46	-0.85	-0.74	-0.82
	(0.182)	(0.007)	(0.033)	(0.007)
NMHC	-0.58	0.27	0.60	0.52
	(0.130)	(0.518)	(0.114)	(0.148)
Ethane	-0.72	0.33	0.43	0.36
	(0.018)	(0.419)	(0.292)	(0.347)
Propane	-0.66	0.24	0.33	0.32
	(0.070)	(0.571)	(0.417)	(0.195)
Ethene	-0.28	-0.61	0.68	0.78
	(0.505)	(0.110)	(0.067)	(0.013)
Propene	-0.63	0.52	0.85	0.89
	(0.105)	(0.195)	(0.007)	(0.004)
Benzene	-0.65	0.45	0.81	0.59
	(0.081)	(0.259)	(0.014)	(0.088)
Toluene	-0.59	0.55	0.86	0.51
	(0.125)	(0.154)	(0.005)	(0.153)

Values in italic type indicate correlations at the 95% confidence level or better.

particles. SEM and TEM analyses show an association between particle aggregates and flaming phase combustion (see section 4.2) [*Martins et al.*, this issue (a)]. In and above the flame zone, temperatures and particle concentrations are high. The coagulation rate is linearly dependent on temperature, on the square of the particle concentration, and roughly inversely proportional to the square of particle diameter. Thus particles with diameters <0.15 μm are highly susceptible to coagulation in and near the flame zone. Freshly nucleated particles and high-temperature condensates should have very short lifetimes before coagulating/condensing with other particles.

This scenario is supported, in part, by the nature of the core particles. As shown in Figure 7, there is a strong positive correlation (0.95) between the core particle CMD and the MCE (*r*=0.95). However, unlike unmodified particles, the VMD or the σ_{gc} for core particles are not correlated with the MCE. This could be due to coagulation decreasing the standard deviation of the particle number distribution.

While there is no significant correlation between the measured particle concentrations and the MCE or particle size parameters, there is a strong negative correlation between the particle volume parameters (VMD and σ_{gc}) and the flux-intensity scale (Table 2). There is also a strong negative

correlation between the NO$_x$ emission factor and the σ_{gc}, as well as a slight (though not statistically significant) positive correlation between the NO$_x$ emission factor and the CMD. Recall that, NO$_x$ can be interpreted as a surrogate for flame temperature. Thus the anticorrelation between the σ_{gc} and the NO$_x$ emission factor may indicate a correlation between σ_{gc} and temperature. The correlation between the flux-intensity scale and the NO$_x$ emission factor with σ_{gc} (Table 2) is to be expected for particles growing by coagulation and condensation at high temperatures.

If condensation and coagulation were the only mechanisms responsible for particle growth, the VMD should increase with the MCE. However, the VMD is negatively correlated with the MCE (albeit not significantly). Also, very strong anticorrelations exist among VMD, the intensity-flux scale, and several emission factors such as NO$_x$ (Table 2). Similarly strong correlations exist between σ_{gv} and these parameters. Thus it appears that while the CMD is governed by flame processes, the VMD may be governed by processes outside the combustion zone.

There are strong correlations between VMD and the emission factors of propene, benzene, and toluene (Table 2). At high temperatures these double-bonded carbon species have accelerated reaction rates. If these unsaturated hydrocarbons survive the combustion process, it is likely that longer chain hydrocarbons also survive. After smoke leaves the combustion zone, it cools rapidly and the longer chain hydrocarbons condense onto the larger particles, thereby increasing the VMD. This interpretation is supported by the positive correlation between the VMD and the aerosol mass emission factor. Thus much of the aerosol mass is likely to be a result of condensation of these hydrocarbons.

Condensational growth of aerosol particles should decrease σ_{gv} [*McMurry and Wilson*, 1982]. Thus if the VMD of the particle size distribution is controlled by condensation, one would expect σ_{gv} to decrease with increasing VMD (and decreasing MCE). However, contrary to this expectation, we found that σ_{gv} increased with decreasing MCE. A similar tendency is seen for σ_{gc}; thus CMD and VMD are anticorrelated. This behavior could be due to several processes. As can be seen from the TEM images in Figure 2, the particles were both internally and externally mixed. Condensation might be favored on specific particle species,
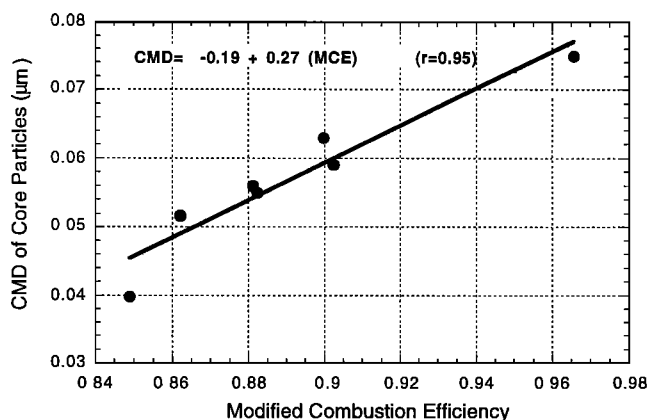
Figure 7. Count median diameter (CMD) of core particle in the accumulation mode for aerosol from forest fires in Brazil versus modified combustion efficiency.

which would widen the particle size distribution. There is also an anticorrelation among the flux-intensity scale, VMD, and σ_{gv}. This suggests that on moving from higher to lower combustion efficiencies, a homogeneous flaming process is replaced by a more heterogeneous (mixed phase) smoldering environment. In many of the fires we studied there were small pockets of combustion that burned at various temperatures and with various combustion efficiencies and combustion rates. Therefore the aerosol in a plume derived from many small subfires. It is not surprising therefore that the aerosol size spectra in such plumes had a broad distribution and a large VMD.

In summary, at least three processes probably govern the aerosol size distribution emitted by a fire. First, the data indicate that the CMD is influenced most heavily by in-flame processes such as high-temperature condensation and coagulation. Second, since the VMD is a function of the emission factor of unsaturated hydrocarbons, it is likely dominated by the condensation of low volatility and long-chain hydrocarbons. Finally, the highly heterogeneous nature of a fire on small scales will likely produce very variable aerosols in a plume.

The magnitudes of the CMD and VMD of the aerosols produced by biomass burning in Brazil are significantly lower than those for North American fires. For example, Radke et al. [1991] measured CMD and VMD of 0.14 and 0.29 μm, respectively, near the source of a flaming wildfire in the Pacific Northwest. Similarly, in the study reported by Hobbs et al. [1997a], CMD values for particles produced by the flaming phase of intense prescribed fires in Washington State were frequently found to be between 0.15 and 0.23 μm. In both of these cases, measurements were performed on very young smoke plumes (<5 min old) using the same UW aircraft facility, instrumentation, and protocols. Thus it is unlikely that these observed differences in particle size are the result of artifact.

There are several possible reasons for the differences between the smoke from fires in Brazil and North America. Firstly, the vegetation is quite different. Also, the sizes of fires studied in North America were much larger than those studied in SCAR-B. For example, in the two North American studies mentioned above, the particle concentrations close to the fires were at least a factor of 4 to 10 greater than those measured in SCAR-B. Thus particle growth by coagulation would be expected to be roughly 16 to 100 times more efficient in the North American plumes than in the plumes studied in SCAR-B. It is also likely that in such very intense fires there is oxygen depravation in the interior flame zone causing significant changes in fire chemistry [Cofer et al., 1997]. In such circumstances, particles would not be fully oxidized and thus may be larger in size. Thus it is not surprising that the smoke from the very large and intense fires in North America is significantly different than that from the smaller fires measured in Brazil.

4.2.2. Grass and cerrado fires. Particle size distributions in plumes from four cerrado and five grass fires were measured with the DMPS. Because the grass and cerrado fuels tended to be dry and small, almost all of the smoke was from flaming combustion, and the MCEs were in the range of 0.89-0.98. Average particle size spectra for grass and cerrado fires are shown in Figures 8a and 8b, respectively. The particle count and volume size distributions varied tremendously.

Grass fires typically had an average CMD and VMD of 0.1 and 0.33 μm, respectively. The CMD follow the same trends that we have described for forest fires, increasing with increasing MCE (r=0.57). However, unlike the forest fires, the VMD for the grass and cerrado fires increased with increasing MCE (r=0.68). These regressions improve significantly if the CE is substituted for the MCE (with r values of 0.73 and 0.74 for the CMD and VMD, respectively).

Cerrado fires typically had the smallest volume median diameter (0.22 μm) of all the fuel types. Also, cerrado fires exhibited the most variation in number distributions, with CMD values clustering around 0.08 and 0.125 μm. In a plot of CMD versus MCE (not shown) the line connecting these two clusters has a negative slope; that is, the particle size decreased with increasing combustion efficiency. Furthermore, the values of the VMD, σ_{gc}, and σ_{gv} for cerrado fires increased with increasing combustion efficiency. These trends are opposite to those for the forest fires.

While the differences between the particle characteristics for the different fuel types are interesting, it must be emphasized that the trends for the grass and cerrado fires are not statistically significant. Correlations between particle moments for grass and cerrado fires and the MCE may be good, but due to the low number of data points, the p values are high.

4.3. Optical Properties of the Smoke Particles

4.3.1. Particle absorption. A summary of our measurements of the absorption characteristics of the smoke aerosols is given in Table 3. For flaming combustion, and for all fuels, the particle mass absorption efficiency (α_a) ranged from 0.7 to 2.0 m^2 g^{-1} and had a mean value of ~1 m^2 g^{-1}. For
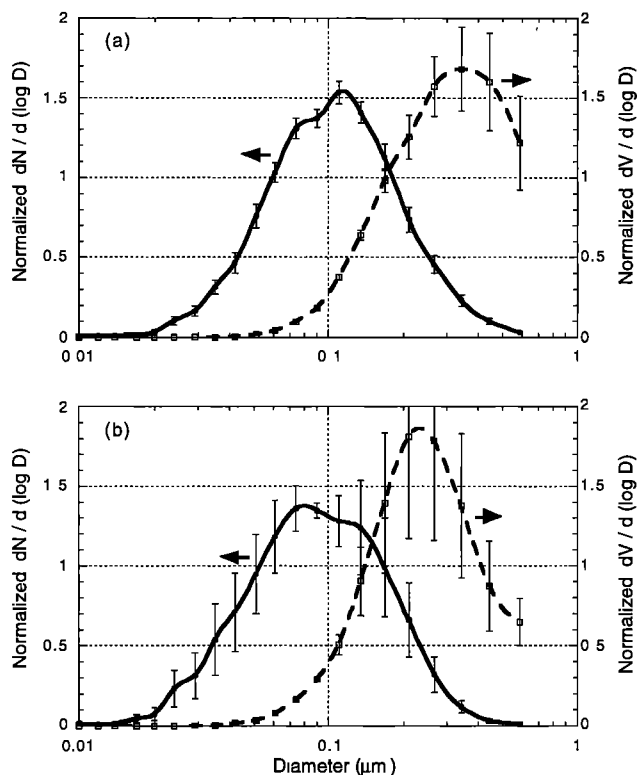
Figure 8. Normalized accumulation mode number (solid lines) and volume (dashed lines) particle size distributions for smoke from (a) grass and (b) cerrado fires in Brazil.

Table 3. Absorption Parameters (Mean ± Standard Error) of Smoke Particles Less Than 4 min Old in Brazil

	Forest			
	Flaming	Smoldering	Grass	Cerrado
Number of samples	5	6	5	6
α_a (m^2 g^{-1} at 550 nm)	1.0 ± 0.2	0.7 ± 0.1	1.1 ± 0.2	1.0 ± 0.1
	No λ Dependence of α_a			
ω_o (450 nm)	0.82 ± 0.05	0.89 ± 0.02	0.81 ± 0.07	0.84 ± 0.03
ω_o (550 nm)	0.74 ± 0.06	0.84 ± 0.02	0.76 ± 0.08	0.77 ± 0.03
ω_o (700 nm)	0.61 ± 0.06	0.73 ± 0.03	0.63 ± 0.10	0.64 ± 0.04
	$1/\lambda$ dependence of α_a			
ω_o (450 nm)	0.79 ± 0.06	0.86 ± 0.02	0.77 ± 0.07	0.81 ± 0.03
ω_o (550 nm)	0.74 ± 0.06	0.84 ± 0.02	0.76 ± 0.07	0.77 ± 0.03
ω_o (700 nm)	0.67 ± 0.06	0.77 ± 0.03	0.68 ± 0.10	0.69 ± 0.04

The wavelength dependence of the single-scattering albedo (ω_o) is presented assuming no wavelength dependence of α_a and a $1/\lambda$ dependence of α_a. The mass absorption efficiency (α_a) was measured with the integrating plate. The two cases when the single-scattering albedo was less than 0.4 are not included in these statistics.

smoldering combustion the mass absorption efficiency ranged from 0.43 to 0.9 m^2 g^{-1}, with a mean value of 0.72 m^2 g^{-1}.

These relatively high α_a values produce low single-scattering albedos (ω_o). The mean values of ω_o, derived from α_a values measured by the integrating plate technique and optical extinction cell (OEC) for grass, cerrado, flaming forest, and smoldering forest fires at a wavelength 538 nm are 0.76, 0.77, 0.74, and 0.84, respectively. Mean ω_o values for each fuel type derived from the OEC and IP were within ±0.01 of each other. Values of ω_o for flaming combustion varied tremendously over the range 0.35-0.9; this was likely due to large variations in particle sizes and compositions. For forest fires there was a fair correlation ($r=0.63$) between ω_o and MCE (Figure 9).

On several occasions, smoke plumes from grass and forest fires had single-scattering albedos <0.4 (based on α_a values measured by all three absorption techniques). Single-scattering albedos this low are near the theoretical limit set by Mie theory for highly absorbing particles with sizes similar to those of smoke particles. In this limit, only diffracted light is scattered. The black carbon content of the aerosol in these cases was 30%, and the MCE was about 95%. It is not known why a few fires emitted such highly absorbing particles.

The largest uncertainty in our absorption measurements is related to the wavelength dependence of α_a for black carbon, which was not directly measured in SCAR-B. Current theoretical estimates of this wavelength dependence range from gray body (i.e., independent of wavelength) to a $1/\lambda$ dependence [*Patterson and McMahon*, 1984; *Foot and Kilsby*, 1989; *Martins et al.*, this issue (b)]. Therefore in Table 3 we list estimates of ω_o using these two extremes, which should yield upper and lower bounds for ω_o. From Table 3, we see that this uncertainty has the largest influence on ω_o at the red wavelength, with a difference of 0.05 between the two extremes.

The ω_o values of smoke particles in Brazil are significantly lower than those measured for fresh smoke (less than 5 min old) from North American fires by *Radke et al.* [1991] and

Hobbs et al. [1997a]. In the latter studies, smoke particles from boreal forest and prescribed fires were found to have a mass absorption efficiency of 0.64±0.35 m^2 g^{-1} and a single-scattering albedo of 0.80-0.95 in the green wavelength, where the single-scattering albedo was derived from measurements using the same OEC used in SCAR-B. The difference in the single-scattering albedos for smoke in Brazil and North America were confirmed using measurements of α_a from the optical reflectance technique [*Reid et al.*, this issue (a)].

The difference in the absorption of smoke particles from fires in Brazil and North America is likely due to the smaller sizes of the smoke particles in Brazil. Electromagnetic theory predicts that if the volume fraction of black carbon in a particle remains constant, the single-scattering albedo should decrease as particle size decreases (this is because there is less scattering due to diffraction at smaller sizes). Furthermore, for
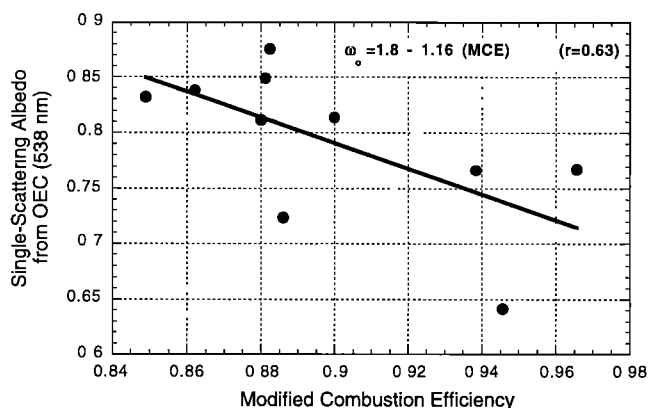
Figure 9. Single-scattering albedo at $\lambda=540$ nm based on α_a measurements from the optical extinction cell (OEC) versus the modified combustion efficiency for flaming and smoldering forest fires in Brazil. One data point (at MCE=0.98, ω_o=0.35) has been omitted because of its large influence on the regression.
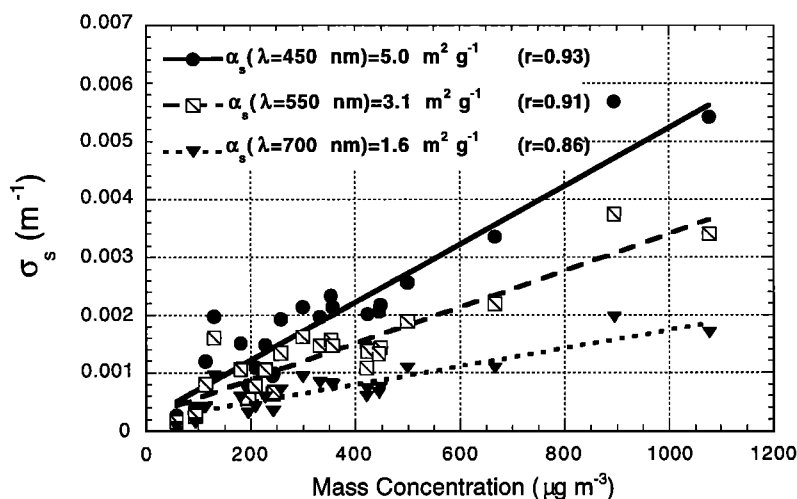
Figure 10. Light-scattering coefficient (σ_s) versus aerosol mass concentration for all fires in Brazil at λ=450 nm (circles), λ=550 nm (squares), and λ=700 nm (triangles). The slope (e.g., 2.9 m^2 g^{-1} for λ=550 nm) is the average particle mass scattering efficiency.

smaller particles, black carbon has a higher mass absorption efficiency [*Martins et al.*, this issue (b)]. Since the mean particle size of smoke from biomass burning in Brazil is smaller than that in North America, this accounts, in part at least, for the higher absorption and lower single-scattering albedo of smoke particles in Brazil.

4.3.2. Particle scattering. By plotting σ_s values against the measured aerosol mass concentration for all samples taken, we can derive the average mass scattering efficiency for smoke aerosols (Figure 10). The regressions are good, with correlations in excess of 0.8 at all three wavelengths. The mass scattering efficiency is highly wavelength dependent, with values of 5.0, 3.1, and 1.6 m^2 g^{-1} at 450, 550, and 700 nm, respectively.

A summary of particle light-scattering measurements by fuel type is given in Table 4. Considerable differences exist for different fuel types and wavelengths. For example, for all fuel types the Angstrom coefficient for 550 to 700 nm are 0.1 to 1 greater than for 450 to 700 nm. Also, the Angstrom coefficients for smoke from forest fires vary by about ±0.2 for flaming and smoldering combustion.

Mean values of the hemispheric backscatter ratio, $\beta(1)$, at a wavelength of 550 nm vary from 0.16 to 0.19. As in the case of the mass scattering efficiency, smoke particles from forest fires exhibit a good correlation $(r>0.6)$ between $\beta(1)$ and the MCE (Figure 11).

Of all the scattering parameters, the mass scattering efficiency showed the greatest variation. For forest fires there

Table 4. Light-Scattering Parameters of Smoke Particles From Various Fires in Brazil

	Forest		Grass	Cerrado
	Flaming	Smoldering		
Number of samples	6	6	6	6
Angstrom coefficient				
(λ=450-550 nm)	2.3 ± 0.1	2.1 ± 0.2	1.4 ± 0.10	2.1 ± 0.1
(λ=550-700 nm)	2.4 ± 0.08	2.6 ± 0.1	2.5 ± 0.06	2.6 ± 0.1
α_s (in m^2 g^{-1} at λ=450 nm)	4.5 ± 0.4	5.5 ± 0.5	4.6 ± 0.6	5.1 ± 0.5
	(3.3-4.9)	(4.0-5.8)	(3.0-7.0)	(2.4-6.7)
α_s (in m^2 g^{-1} at λ=550 nm)	2.8 ± 0.5	3.6 ± 0.4	3.5 ± 0.5	3.4 ± 0.6
	(2.2-3.3)	(2.8-4.4)	(2.4-5.1)	(1.7-4.7)
α_s (in m^2 g^{-1} at λ=700 nm)	1.6 ± 0.3	1.9 ± 0.3	1.9 ± 0.3	1.8 ± 0.3
	(1.2-1.8)	(1.5-2.4)	(1.4-2.8)	(0.8-2.5)
$\beta(1)$ (at λ=450 nm)	0.16 ± 0.02	0.15 ± 0.01	0.15 ± 0.02	0.19 ± 0.01
$\beta(1)$ (at λ=550 nm)	0.20 ± 0.01	0.16 ± 0.01	0.17 ± 0.02	0.21 ± 0.01
$\beta(1)$ (at λ=700 nm)	0.23 ± 0.02	0.19 ± 0.01	0.19 ± 0.02	0.23 ± 0.01

Listed are the mean ± the standard error of the angstrom coefficient, the mass scattering efficiency (α_s), and the backscatter ratio $(\beta(1))$. Given in parentheses are the range of values of α_s in which 95% of the measurements occurred.
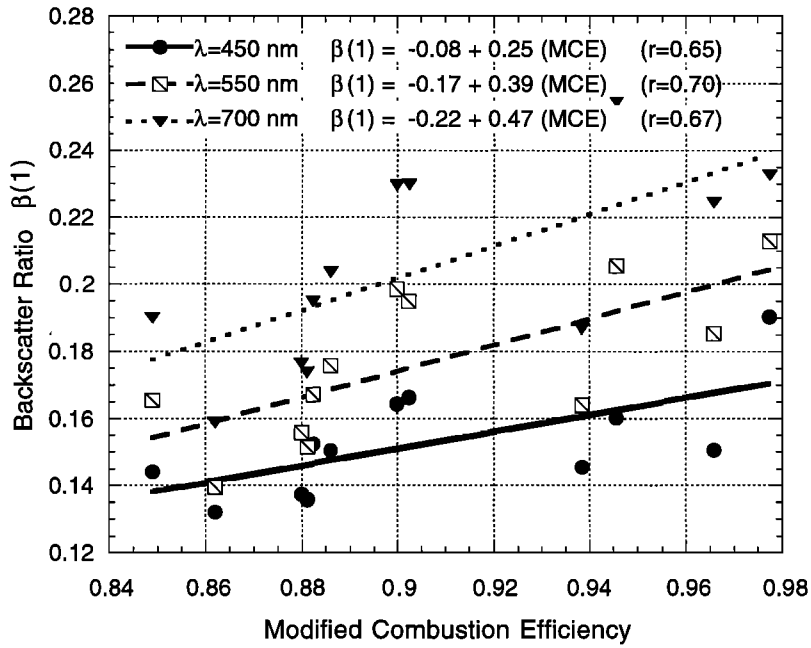
Figure 11. Aerosol backscatter ratio $\beta(1)$ at λ=450, 550, and 700 nm versus the modified combustion efficiency for flaming and smoldering forest fires in Brazil.

is a statistically significant decrease in α_s with increasing MCE (Figure 12).

Large standard errors are usually associated with the measurement of α_s. There are several possible reasons for this. First, α_s is strongly dependent on the aerosol size distribution. At wavelengths of 450 and 550 nm, the derivative of the particle scattering efficiency, Q_{scat}, with respect to particle size is steepest in the range where the submicron mode exists for particles from biomass burning. As discussed earlier, there was a fair amount of variance in the particle volume size distributions, particularly for the grass and cerrado fires. Second, much of the variability in α_s for the data presented here is likely due the difficulty of coordinating the light-scattering measurement with the grab-bag samples
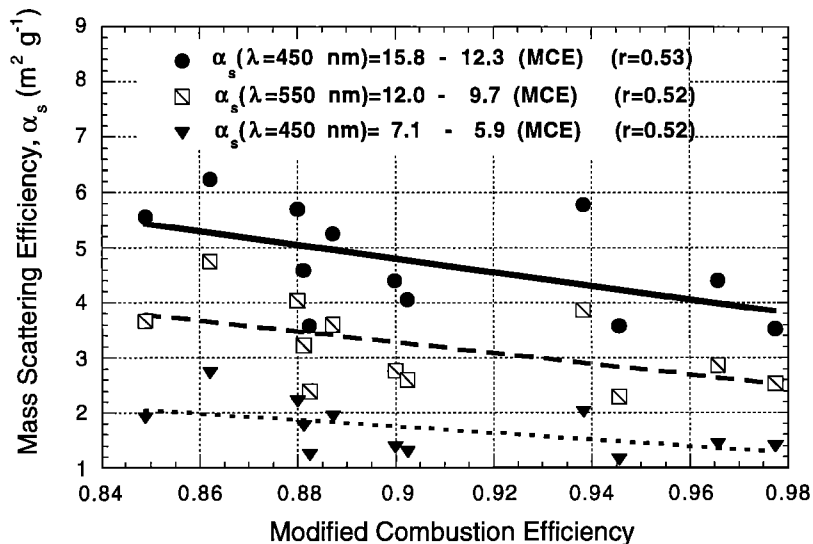
(from which aerosol mass was determined) in a smoke plume. We estimate that as much as 40% of the standard deviation in α_s derives from this uncertainty.

As a test, we generated estimates of α_s from the OEC using the relation

$$\omega_o = \frac{\sigma_s}{\sigma_s + \sigma_a} = \frac{\alpha_s}{\alpha_s + \alpha_a} \tag{9}$$

Then, solving for α_s,

$$\alpha_s = \frac{\omega_o \alpha_a}{(1 - \omega_o)} \tag{10}$$

Figure 12. Aerosol mass scattering efficiency α_s versus the modified combustion efficiency for flaming and smoldering forest fires in Brazil at λ=450 nm (circles), λ=550 nm (squares), and λ=700 nm (triangles).

Using the measured value of ω_o from the OEC and α_a from the integrating plate in (10), yields values for α_s for smoke from cerrado, grass, flaming forest, and smoldering forest fires of 3.2, 3.4, 2.8, and 3.5 m^2 g^{-1}, respectively, at a wavelength of 550 nm. These values are within 0.2 m^2 g^{-1} (or <10%) the mean values of α_s given in Table 4, which were derived from σ_s and particle mass measurements. While this is not a completely independent verification of the scattering measurement (there is a mass measurement in the determination of both α_s and α_a), it does demonstrate that the absorption and scattering measurements are consistent with each other.

The measured values of α_s for smoke from forest fires in Brazil are 0.4 to 1.0 m^2 g^{-1} less than those measured for smoke from North American forest fires. For fresh smoke from prescribed fires in Washington State (less than 5 min old), *Hobbs et al.* [1997a] report a mean value for α_s of 3.7 m^2 g^{-1}, compared to the mean value of 3.1 m^2 g^{-1} for Brazil reported in the present paper. *Radke et al.* [1988, 1991] report average values of α_s ranging from 3.1 to 3.8 m^2 g^{-1} for fresh smoke in the Pacific Northwest. *Tangren* [1982] reported a mean value for α_s of 3.6 m^2 g^{-1} for forest fires in Florida and Georgia. Part of this difference is accounted for by noting that the lowest *MCE* we measured for forest fires in Brazil was 0.84. Other studies, such as those by Radke et al., contain data from fires with *MCE* values as low as 0.75. We see from Figure 11 that our regression line gives a value for α_s of 4.0 m^2 g^{-1} at an *MCE* of 0.84, compared to our mean smoldering value of 3.6 m^2 g^{-1}.

This sampling bias does not account for the low mean values of α_s found for flaming forest combustion in Brazil. Smoke from forest burning in Brazil had higher-absorption coefficients; increased absorption by particles in this size range can occur at the expense of scattering. Finally, the VMD values we measured for smoke from forest fires in Brazil are roughly 0.04 µm smaller than those measured in North America. This, in itself, can reduce the value of α_s by 0.5 m^2 g^{-1} at a wavelength of 550 nm.

In Brazil we measured α_s values at 550 nm for smoke from grass and cerrado fires of 3.5 and 3.4 m^2 g^{-1}, respectively. *Evans et al.* [1976] and *Vines et al.* [1971] measured mean values of α_s for smoke from Australian brush fires that ranged from 3.1 to 4.0 m^2 g^{-1}. Given that the standard error in the mean of our measurements is ± 0.4 m^2 g^{-1}, our values are not statistically different from the Australian grass fire measurements.

4.3.3. Closure studies.

We will now explore the extent to which the optical parameters of the smoke we measured in Brazil are described by Mie theory. This exercise has three primary purposes. First, we wish to determine if our measurements of the sizes and optical parameters of the smoke are consistent with each other. Second, we hope to gain insights into the mechanics and chemistry of the smoke particles. Finally, in view of the complex morphology of the fine-mode smoke particles, we wish to determine the extent to which Mie theory can predict the optical properties of the smoke aerosol.

We begin by performing a correlation analysis of our measured parameters for smoke from the forest fires. Table 5 lists correlation coefficients and p values for all the optical parameters at a wavelength of 550 nm, the *MCE*, the particle size parameters, and some emission factors. Overall, the correlations between the parameters behave as expected. For

example, as the Angstrom coefficients can be interpreted as the slope of a Junge size distribution on a log-log plot, they should be (and are) anticorrelated with σ_{gc} and σ_{gv}. There is also a good correlation among the backscatter ratio, $\beta(1)$, and the VMD (Figure 13). For the particle size regime containing most of the smoke particles, $\beta(1)$ is strongly dependent on particle size. Mie theory predicts that as particles get larger, they scatter more light in the forward direction. As expected, there is a very strong anticorrelation (>-0.80) between the $\beta(1)$ and the σ_{gc}, and the VMD and the σ_{gc}. Because the CMD and σ_{gc} are anticorrelated, there is a weak positive correlation between the $\beta(1)$ and the CMD. Similar and equally strong correlations exist for these parameters for blue and red wavelengths.

The particle mass scattering efficiency α_s is not well correlated with the particle size parameters, but it is strongly correlated with the Angstrom coefficient and $\beta(1)$. The single-scattering albedo correlates better with the particle size parameters and with $\beta(1)$ (r >0.55) than it does with the BC emission factor or even with the BC content of the aerosol (r <0.4). This is in partial agreement with Mie theory, which predicts that particle size should have an important effect on the single-scattering albedo.

In almost all cases, the optical parameters of the aerosol correlate better with the emission factors of unsaturated hydrocarbons than they did with the particle size distribution parameters or the combustion efficiency. This is due, in part, to the fact that in a smoke plume it is easier to measure the emission factors for hydrocarbons than it is to measure the size distribution of the particles. As discussed above, the particle VMD correlated better with the emission factors for unsaturated hydrocarbons than it did with the combustion efficiency. Thus the high correlation between the unsaturated hydrocarbons and the optical parameters may simply indicate that there is less variance in our hydrocarbon measurements than there is in our particle sizing measurements. The high correlation between the hydrocarbon emission factors and the optical parameters also may be indicative of a change in particle composition. As discussed above, high emission factors for unsaturated hydrocarbons probably indicate high emission factors for condensates. Thus when the emission factors for unsaturated hydrocarbons are high, particles may grow more by condensation, which can change their refractive index, black carbon content, and morphology. These changes would manifest themselves as changes in the optical properties of the aerosol.

To shed light on these results, Mie calculations were carried out using the particle lognormal volume distribution parameters given in Table 1. Because coarse particles did not contribute significantly to the measured scattering and absorption measurements, they were excluded from this analysis. From our DMPS measurements the particle density was assumed to be 1.35 g cm^{-3}. Black carbon constituted 7.5 and 5% of the particle mass for flaming and smoldering phase smoke, respectively [*Ferek et al.*, this issue]. On the basis of the TEM micrographs it was assumed that all of the black carbon was internally mixed.

Since there are no direct measurement of the indices of refraction of particles from biomass burning, most authors have assumed a refractive index for the black carbon component similar to acetylene soot, and the outer shell of the biomass-burning aerosol has been assumed to have a refractive index similar to organic aerosols. Indices of refraction for

Table 5. Correlations and p Values (in Parentheses) of Optical Parameters With Each Other and With MCE, Some Particle Size Parameters, and Some Emission Factors for All Forest Fires Analyzed in Brazil

|	Angstrom Coefficient		$\beta(1)$	α_s	ω_o
	450-550 nm	550-700 nm	(at λ=550 nm)	(at λ=550 nm)	(at λ=550 nm)
Angstrom Coefficient					
(λ=450-550 nm)	1	*0.97*	0.56	*-0.63*	0.13
	-	(0.000)	(0.060)	(0.027)	(0.691)
(λ=550-700 nm)	*0.97*	1	*0.608*	*-0.67*	0.07
	(0.000)	-	(0.036)	(0.016)	(0.827)
$\beta(1)$ (at λ=550 nm)	0.56	*0.601*	1	*-0.80*	*-0.73*
	(0.060)	(0.036)	-	(0.002)	(0.011)
α_s (at λ=550 nm)	*-0.63*	*-0.67*	*-0.80*	1	0.39
	(0.027)	(0.016)	(0.002)	-	(0.232)
ω_o (at λ=550 nm)	0.13	0.07	*-0.73*	0.39	1
	(0.691)	(0.827)	(0.010)	(0.232)	-
MCE	0.21	0.34	*0.70*	-0.52	*-0.73*
	(0.495)	(0.280)	(0.011)	(0.082)	(0.011)
CMD	0.55	0.62	0.59	-0.39	-0.52
	(0.127)	(0.072)	(0.091)	(0.296)	(0.186)
σ_{gc}	-0.52	-0.64	*-0.80*	0.49	0.62
	(0.149)	(0.061)	(0.010)	(0.184)	(0.097)
VMD	*-0.72*	*-0.74*	*-0.83*	0.43	0.66
	(0.028)	(0.022)	(0.005)	(0.241)	(0.074)
σ_{gv}	*-0.68*	*-0.71*	*-0.86*	0.57	0.64
	(0.028)	(0.023)	(0.001)	(0.084)	(0.063)
Emission Factors					
Aerosol	0.06	0.02	-0.56	0.04	*0.73*
	(0.850)	(0.959)	(0.059)	(0.883)	(0.011)
BC	-0.17	-0.24	-0.46	0.037	0.37
	(0.590)	(0.454)	(0.130)	(0.907)	(0.257)
NO$_x$	*0.73*	*0.78*	*0.62*	-0.56	-0.15
	(0.011)	(0.004)	(0.043)	(0.072)	(0.680)
Propene	*0.78*	*0.80*	*0.77*	0.69	0.60
	(0.013)	(0.004)	(0.015)	(0.062)	(0.114)
Benzene	*0.85*	*0.86*	*0.81*	*0.76*	0.61
	(0.007)	(0.006)	(0.003)	(0.016)	(0.059)

Correlations equal to or better than the 95% confidence level are shown in italic type. In this table, $\beta(1)$ is the backscatter ratio, α_s is the mass scattering efficiency, ω_o is the single-scattering albedo, CMD is the count median diameter, σ_{gc} is the geometric standard deviation of the number distribution, VMD is the volume median diameter, and σ_{gv} is the geometric standard deviation of the volume distribution.

black carbon can range from 1.75-0.44i to 2.0-1.0i [*Chang and Charalampopoulos*, 1990; *D'Almeida et al.*, 1991; *Martins et al.*, 1997, this issue (a)]. Assumed values for the index of refraction of the shell surrounding the core of the particles vary from 1.4 to 1.6 [*D'Almeida et al.*, 1991; *Martins et al.*, 1997, this issue (a); *Anderson et al.*, 1996; *Remer et al.*, this issue]. We used midrange values for the indices of refraction. Thus the black carbon and the organic shell were assumed to have indices of refraction of 1.8-0.7i and 1.5-0i, respectively. Sensitivity studies were carried out by adjusting the real and complex indices of refraction of the black carbon by ±0.05 and adjusting the real index of refraction of the shell by ±0.05.

Some of the results of the Mie calculations are shown in Table 6. Most of the calculated values at a wavelength of 550 nm are either within or near the standard errors in the measurements. For example, the calculated and observed mass absorption efficiencies and single-scattering albedos for all fuel types compare well. Similarly, the mass scattering efficiency calculations for smoldering phase and grass fire smoke in the green wavelength match the observations nearly perfectly. The measured mass scattering efficiency for flaming forest and cerrado fires is somewhat off the mark but within the standard error of both the measurement and the calculation.

This closure study demonstrates the sensitivity of Mie theory to the values used for the particle parameters. It is likely that the index of refraction of biomass-burning aerosol depends on combustion efficiency, fuel type, and fire intensity. We found that varying the index of refraction of the particle coating by ±0.05 produced a ±0.5 m^2 g^{-1} change in the derived mass scattering efficiency. Similarly, changing the complex index of refraction of black carbon by ±0.05 changed the mass absorption efficiency by 0.1 m^2 g^{-1} and the single-scattering albedo by 0.02. However, these variations are of similar magnitude to the variability in our measurements. Thus even if the theoretical model was refined,
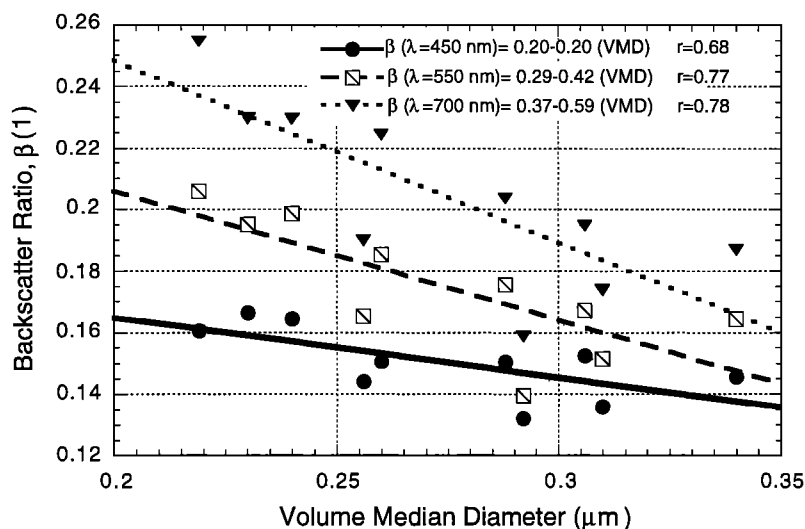
Figure 13. Aerosol backscatter ratio (at three wavelengths) versus particle volume median diameter for forest fires in Brazil.

limitations in current measurement techniques would limit the evaluation of the model.

Despite the successes in using simplified particle morphologies in Mie theory to predict the optical properties of smoke aerosols, there are two notable deficiencies. First, there is some trouble in predicting the wavelength dependence of the total light scattering. Second, Mie theory always overpredicts the value of $\beta(1)$.

For both of the wavelength ranges used here, Mie theory underpredicts the value of the Angstrom coefficient. Thus the measured mass scattering efficiency at a wavelength of 700 nm

is roughly 20% less than predicted by Mie theory. At the 450 nm wavelength the measured mass scattering efficiency is between 0 and 20% higher than predicted. There are several possible explanations for these results. First, it is conceivable that the index of refraction of the particle decreases with increasing particle size. Organic compounds may preferentially exist in the larger sizes, since the larger particles are less oxidized in the flame. Second, it is possible that the black carbon is not evenly distributed across all particle sizes. By using the preheater on the DMPS we know the size distribution of the core particles, but we do not know

Table 6. Observed and Calculated Optical Parameters for Grass, Cerrado, and Forest Fires in Brazil

	Forest			
	Flaming	Smoldering	Grass	Cerrado
Particle volume median diameter	0.26 ± 0.01	0.29 ± 0.01	0.30 ± 0.04	0.23 ± 0.02
Geometric standard deviation (σ_{gv})	1.62 ± 0.07	1.84 ± 0.04	1.87 ± 0.07	1.80 ± 0.14
Angstrom Coefficient λ=450-550 nm				
measured	2.3 ± 0.1	2.1 ± 0.2	1.4 ± 0.1	2.1 ± 0.1
modeled	1.9 ± 0.1	1.6 ± 0.1	1.5 ± 0.1	1.9 ± 0.1
λ=550-700 nm				
measured	2.4 ± 0.1	2.6 ± 0.1	2.5 ± 0.1	2.6 ± 0.1
modeled	2.2 ± 0.1	1.9 ± 0.1	1.8 ± 0.1	2.2 ± 0.1
α_a (in m^2 g^{-1} at λ=550 nm)				
measured	1.0 ± 0.2	0.7 ± 0.1	1.1 ± 0.2	1.0 ± 0.1
modeled	1.0 ± 0.1	0.7 ± 0.1	1.0 ± 0.1	0.9 ± 0.1
ω_0 (at λ=550 nm)				
measured	0.74 ± 0.06	0.84 ± 0.02	0.76 ± 0.08	0.77 ± 0.03
modeled	0.76 ± 0.03	0.84 ± 0.02	0.78 ± 0.02	0.74 ± 0.02
α_s (in m^2 g^{-1} at λ=550 nm)				
measured	2.8 ± 0.5	3.6 ± 0.4	3.5 ± 0.5	3.4 ± 0.6
modeled	3.1 ± 0.6	3.5 ± 0.6	3.4 ± 0.5	2.7 ± 0.5
$\beta(1)$ (at λ=550 nm)				
measured	0.20 ± 0.01	0.16 ± 0.01	0.17 ± 0.02	0.21 ± 0.01
modeled	0.15 ± 0.02	0.14 ± 0.02	0.14 ± 0.02	0.17 ± 0.02

the thickness of the organic coatings. Third, it is possible that the complicated structure of a biomass-burning aerosol has a significant effect on the scattering characteristics of the particles.

From Table 6 it is also clear that Mie theory consistently predicts a value for $\beta(1)$ that is 0.02 to 0.05 higher than measured. A series of tests were carried out to examine the sensitivity of $\beta(1)$ to the input parameters. Variations in black carbon content and indices of refraction had little effect on $\beta(1)$. Even variations in the distribution of black carbon and the index of refraction with particle size had only modest effects, producing changes in $\beta(1)$ of <0.02. The only way to significantly increase the value of $\beta(1)$ was to decrease VMD of the particles by 0.04 μm. As discussed earlier, there are differences in the VMD values derived from the optical probes and the DMPS. It is possible that DMPS measurements overestimated particle sizes. However, if the VMD is reduced, the calculated mass scattering efficiency is drastically decreased, which worsens the comparison between the measured and the calculated wavelength dependence of the total light scattering.

Differences between the measured values of $\beta(1)$ and those predicted from particle size distributions by Mie theory have been noted for a variety of aerosol types [Kiel and Briegleb, 1993; Quinn et al., 1995; and Ross et al., this issue]. The reasons for this are not clear. It is fairly easy to measure $\beta(1)$, and in our measurements, it correlates very well with the aerosol size distribution parameters and other optical properties (Table 5). However, it is possible that there is a systematic error due to flaws in the nephelometer design. It is also possible that for the purpose of calculating $\beta(1)$ there is some deficiency in the application of Mie theory.

5. Conclusions

Particles produced by forest fires in Brazil correlate well with fire intensity and certain emission factors. However, the MCE may not be so good a predictor of the emission factor and characteristics of smoke particles as it is for gaseous emissions. Three processes appear to govern the particle size distributions in the smokes. First, the high positive correlation between the CMD and the fire combustion efficiency suggests that the CMD is influenced most strongly by in-flame processes, such as high-temperature condensation and coagulation. Second, since the VMD is not a strong function of the MCE but is highly correlated with the emission factors of unsaturated hydrocarbons such as alkenes and aromatics, and in view of the positive correlation of the VMD with the aerosol mass emission factor, the VMD may be controlled by the condensation of low volatility and long-chain hydrocarbons. Finally, smoke from smoldering and mixed-phase fires in this study arose from many small pockets of combustion which burned with various degrees of efficiency, which gave rise to a broad particle size distribution. This effect was greater than the tendency of aerosol condensation and coagulation to decrease the width of the particle spectra.

Large variations in the size distributions of smoke particles produced large variations in their optical properties. Smokes from forest fires in Brazil absorbed more and scattered less solar radiation than smoke from biomass burning in North America. This is likely due to the smaller particle sizes of smoke in Brazil. The optical properties of smoke from grass

and cerrado fires in Brazil are similar to those measured in other locations.

Despite the complicated internal structure of fine-mode smoke particles, Mie theory applied to particles assumed to have a central absorbing core coated with organics did reasonably well in predicting the particle optical properties. The measured mass scattering efficiency at wavelengths of 450, 550, and 700 nm were generally within 20% of values predicted by Mie theory. However, the wavelength dependence of the aerosol mass scattering efficiency and the backscatter ratio were only fairly reproduced by Mie theory. These discrepancies may be compensated for in part by adjusting the assumed index of refraction and black carbon content of particles with size. However, the reason for the consistent discrepancy between the measurement of the backscatter ratio and the Mie theory is unclear.

References

Anderson, B. E., W. B. Grant, G. L. Gregory, E. V. Browell, J. E. Collins Jr., D. W. Sachse, D. R. Bagwell, C. H. Hudgins, D. R. Blake, and N. J. Blake, Aerosols from biomass burning over the tropical South Atlantic region: Distributions and impacts, J. Geophys. Res., 101, 24,117-24,137, 1996.

Andreae, M. O., Biomass burning: Its history, use, and distribution and its impact on environmental quality and global climate, in Biomass Burning and Global Change, edited by J. S. Levine, pp. 3-21, MIT Press, Cambridge, Mass., 1991.

Artaxo, P., F. Gerab, M. A. Yamasoe, and J. V. Martins, Fine mode aerosol composition at three long-term atmospheric monitoring sites in the Amazon Basin, J. Geophys. Res., 99, 22,857-22,868, 1994.

Cachier, H., M. P. Brémond, and P. Buat-Ménard, Determination of atmospheric soot carbon with a simple thermal method, Tellus, Ser. B., 41, 379-390, 1989.

Chandler, C., P. Cheney, P. Thomas, L. Trabaud, and D. Williams, Fire in Forestry, vol. 1, John Wiley, New York, 1983.

Chang, H., and T. T. Charalampopoulos, Determination of the wavelength dependence of refractive indices of flame soot, Proc. R. Soc. London, Ser. A, 430(1880), 577-591, 1990.

Cofer, W. R., III, E. L. Winstead, B. J. Stocks, L. W. Overbay, J. G. Goldammer, D. R. Cahoon, and J. S. Levine, Emissions from boreal forest fires: Are the atmospheric impacts underestimated?, in Biomass Burning and Global Change, edited by J. S. Levine, pp. 834-839, MIT Press, Cambridge, Mass., 1997.

Coutinho, L. M., Fire in the ecology of the cerrado, in Fire in the Tropical Biota (Ecological Studies 84), edited by J. G. Goldammer, pp. 82-105, Springer-Verlag, New York, 1990.

D'Almeida, G. A., K. Koepke, and E. R. Shettle, Atmospheric Aerosols: Global Climatology and Radiative Characteristics, A. Deepack, Hampton, Va., 1991.

Einfeld, W., D. E. Ward, and C. Hardy, Effects of fire behavior on prescribed fire smoke characteristics: A case study, in Biomass Burning and Global Change, edited by J. S. Levine, pp. 412-419, MIT Press, Cambridge, Mass., 1991.

Evans, L. F., N. K. King, D. A. MacArthur, D. R. Packham, and E. T. Stephens, Further studies on the nature of brushfire smoke, Div. Appl. Org. Tech. Pap. 2, CSIRO, Atmos. Res., Aspendale, Victoria, Australia, 1976.

Fearnside, P.M., Fire in the tropical rain forest of the Amazon Basin, in Fire in the Tropical Biota (Ecological Studies 84), edited by J. G. Goldammer, pp. 106-115, Springer-Verlag, New York, 1990.

Fearnside, P.M., Greenhouse gas contributions from deforestation in

Brazilian Amazonia, in *Global Biomass Burning: Atmospheric, Climatic, and Biospheric Implications*, edited by J. S. Levine, pp. 92-105, MIT Press, Cambridge, Mass., 1991.

Ferek, R. J., J. S. Reid, P. V. Hobbs, D. R. Blake, and C. Liousse, Emission factors of hydrocarbons, halocarbons, trace gases, and particles from biomass burning in Brazil, *J. Geophys. Res.*, this issue.

Foot, J. S., and C. G. Kilsby, Absorption of light by aerosol particles: An intercomparison of techniques and spectral observations, *Atmos. Environ., 23*, 489-495, 1989.

Glassman, I., Soot formation in combustion processes, in *Twenty-Second Symposium (International) on Combustion*, 295 pp., The Combust. Inst., Pittsburgh, Pa., 1988.

Hegg, D. A., D. S. Covert, M. J. Rood, and P. V. Hobbs, Measurements of aerosol optical properties in marine air, *J. Geophys. Res., 101,* 12,893-12,903, 1996.

Hobbs, P. V., Summary of types of data collected on the University of Washington's Convair C-131A aircraft in the Smoke, Clouds and Radiation-Brazil (SCAR-B) field study from 17 August-20 September 1995, Report from the Cloud and Aerosol Research Group, Dep. of Atmos. Sci., Univ. of Washington, Seattle, March 1996. (Also available on http://cargsun2.atmos.washington.edu/.)

Hobbs, P. V., J. S. Reid, J. A. Herring, J. D. Nance, R. E. Weiss, J. L. Ross, D. A. Hegg, R. D. Ottmar, and C. A. Liousse, Particle and trace-gas measurements in the smoke from prescribed burns of forest products in the Pacific Northwest, in *Biomass Burning and Global Change*, edited by J. S. Levine, pp. 697-715, MIT Press, Cambridge, Mass., 1997a.

Hobbs, P. V., J. S. Reid, R. A. Kotchenruther, R. J. Ferek, and R. Weiss, Direct radiative forcing by smoke from biomass burning, *Science, 275*, 1776-1778, 1997b.

Intergovernmental Panel on Climate Change (IPCC), *Climate Change 1995: The Science of Climate Change*, edited by J. T. Houghton et al., Cambridge Univ. Press, New York, 1996.

Kaufman Y. J., C. J. Tucker, and I. Fung, Remote sensing of biomass burning in the tropics, *J. Geophys. Res., 95*, 9927-9939, 1990.

Kent, J. H., A quantitative relationship between soot yield and smoke point measurements, *Combustion and Flame, 63*, 349-358, 1986.

Kiel, J. T., and B. P. Briegleb, The relative roles of sulfate aerosols and greenhouse gases in climate forcing, *Science, 260*, 311-314, 1993.

Kotchenruther, R. A., and P. V. Hobbs, Humidification factors of aerosols from biomass burning in Brazil, *J. Geophys. Res.*, this issue.

Lin, C., M. Baker, and R. Charlson, Absorption coefficient of atmospheric aerosols: A method for measurement, *Appl. Opt., 12*, 1356-1363, 1973.

Liousse, C., C. Devaux, F. Dulac, and H. Cachier, Aging of savannah biomass burning aerosols: Consequences on their optical properties, *J. Atmos. Chem., 22*, 1-17, 1995.

Lobert, J. M., and J. Warnatz, Emissions from the combustion process in vegetation, in *Fire in the Environment: The Ecological, Atmospheric and Climatic Importance of Vegetation Fires*, edited by P. J. Crutzen and J. G. Goldammer, pp. 15-37, John Wiley, New York, 1993.

Martins, J. V., P. Artaxo, P. V. Hobbs, C. Liousse, H. Cachier, Y. Kaufman, and A. Plana-Fattori, Particle size distributions, elemental compositions, carbon measurements, and optical properties of smoke from biomass burning in the Pacific Northwest of the United States, in *Biomass Burning and Global Change*, edited by J. S. Levine, pp. 716-732, MIT Press, Cambridge, Mass., 1997.

Martins, J. V., P. V. Hobbs, R. E. Weiss, and P. Artaxo, Sphericity and morphology of smoke particles from biomass burning in Brazil, *J. Geophys. Res.*, this issue (a).

Martins, J. V., P. Artaxo, C. Liousse, J. S. Reid, P. V. Hobbs, and Y. Kaufman, Effects of black carbon content, particle size, and mixing on light absorption by aerosol from biomass burning in Brazil, *J. Geophys. Res.*, this issue (b).

McMurry, P. H., and J. C. Wilson, Growth laws for the formation of secondary ambient aerosols: Implications for chemical conversion mechanisms, *Atmos. Environ., 16*, 121-132, 1982.

Patterson, E. M., and C. K. McMahon, Absorption characteristics of forest fire particulate matter, *Atmos. Environ., 18*, 2541-2551, 1984.

Penner, J. E., R. Dickinson, and C. O'Neil, Effects of aerosol from biomass burning on the global radiation budget, *Science, 256*, 1432-1434, 1992.

Pyne, S., *Introduction to Wildland Fires: Fire Management in the United States*, pp. 1-34, John Wiley, New York, 1984.

Quinn, P. K., S. F. Marshall, T. S. Bates, D. S. Covert, and V. N. Kapustin, Comparison of measured and calculated aerosol properties relevant to the radiative forcing of tropospheric sulfate aerosol on climate, *J. Geophys. Res., 100*, 8977-8991, 1995.

Radke, L. F, D. A. Hegg, J. H. Lyons, C. A. Brock, P. V. Hobbs, R. Weiss, and R. Rassmussen, Airborne measurements on smokes from biomass burning, in *Aerosols and Climate*, edited by P. V. Hobbs and M. P. McCormick, pp. 411-422, A. Deepak, Hampton, Va., 1988.

Radke, L. F., D. A. Hegg, P. V. Hobbs, J. D. Nance, J. H. Lyons, K. K. Laursen, R. E. Weiss, P. J. Riggen, and D. E. Ward, Particulate and trace emissions from large biomass fires in North America, in *Global Biomass Burning: Atmospheric, Climatic, and Biospheric Implications*, edited by J. S. Levine, pp. 209-224, MIT Press, Cambridge, Mass., 1991.

Reid, J. S., T. A. Cahill, P. H. Wakabayashi, and M. R. Dunlap, Geometric/aerodynamic equivalent diameter ratios of ash aggregate aerosols collected in burning Kuwaiti well fields, *Atmos. Environ., 28*, 2227-2234, 1994.

Reid, J. S., P. V. Hobbs, R. J. Ferek, J. V. Martins, D. Blake, M. R. Dunlap, and C. Liousse, Physical, chemical and optical properties of regional hazes dominated by smoke in Brazil, *J. Geophys. Res.*, this issue (a).

Reid, J. S., P. V. Hobbs, C. Liousse, J. V. Martins, R. E. Weiss, and T. F. Eck, Comparisons of techniques for measuring shortwave absorption and the black carbon content of biomass burning aerosols, *J. Geophys. Res.*, this issue (b).

Remer, L. A., Y. J. Kaufman, B. N. Holben, A. M. Thompson, and D. McNamara, Biomass burning aerosol size distribution and modeled optical properties, *J. Geophys. Res.*, this issue.

Robock, A., Surface Cooling due to forest fire smoke, *J. Geophys. Res., 96*, 20,869-20,878, 1991.

Ross, J. L., P. V. Hobbs, and B. Holben, Radiative characteristics of regional hazes dominated by smoke from biomass burning in Brazil: Closure tests and direct radiative forcing, *J. Geophys. Res.*, this issue.

Scorer, R. S., *Environmental Aerodynamics*, John Wiley, New York, 1978.

Tangren, C.D., Scattering coefficient and particulate matter concentration in forest fire smoke, *J. Air Pollut. Control Assoc., 32*, 729-732, 1982.

Turns, S. R., *An Introduction to Combustion, Concepts and Applications*, pp. 291-297, McGraw-Hill, New York, 1996.

Vines, R. G., L. Gibson, A. B. Hatch, N. K. King, D. A. MacArthur, D. R. Packham, and R. J. Taylor, On the nature, properties and behavior of brush fire smoke, *Div. Appl. Chem., Tech. Pap. 1*, Commonw. Sci. and Ind. Res. Organ., Melbourne, Australia, 1971.

Ward, D. E., Factors influencing the emissions of gases and particulate matter from biomass burning, in *Fire in the Tropical Biota (Ecological Studies 84)*, edited by J. G. Goldammer, pp. 418-436, Springer-Verlag, New York, 1990.

Ward, D. E., and W. M. Hao, Air toxic emissions from burning of biomass globally—Preliminary estimates, in *Proceedings of the 85th Annual Meeting and Exhibition*, Air and Waste Management Association, 1992.

Ward, D. E., and C. C. Hardy, Smoke emissions from wildland fires, *Environ. Intern., 17*, 117-134, 1991.

Ward, D. E., A. W. Setzer, Y. J. Kaufman, and R. A. Rasmussen, Characteristics of smoke emissions from biomass fires of the Amazon region-BASE-A experiment, in *Biomass Burning and Global Change*, edited by J. S. Levine, pp. 394-402, MIT Press, Cambridge, Mass., 1991.

Ward, D. E., R. A. Susott, J. B., Kaufman, R. E. Babbit, D. L. Cummings, B. Dias, B. N. Holben, Y. J. Kaufman, R. A. Rasmussen, and A. W. Setzer, Smoke and fire characteristics for cerrado and deforestation burns in Brazil: Base B Experiment, *J. Geophys. Res., 97*, 14,601-14,619, 1992.

Weiss, R. E., and P. V. Hobbs, Optical extinction properties of smoke from the Kuwait oil fires, *J. Geophys. Res., 97*, 14,537-14,540, 1992.

Westphal, D. L., and O. B. Toon, Simulations of microscale, radiative, and dynamical processes in a continental-scale forest fire smoke plume, *J. Geophys. Res., 96*, 22,379-22,400, 1991.

Winklmayer, W., G. P. Reischl, A. O. Lindner, and A. Berner, A new electromobility spectrometer for the measurement of the aerosol size distributions in the size ranges of 1 to 1,000 nm, *J. Aerosol Sci., 22*, 289-296, 1991.

P. V. Hobbs (corresponding author) and J. S. Reid, Department of Atmospheric Sciences, University of Washington, Box 351640, Seattle, WA 98195-1640. (e-mail: phobbs@atmos.washington.edu; jreid@spawar.navy.mil.)